Perceptual decision making: Biases in post-error reaction times explained by attractor network dynamics

Kevin Berlemont, Jean-Pierre Nadal

Perceptual decision making: Biases in post-error reaction times explained by attractor network dynamics

Kevin Berlemont[1], **and Jean-Pierre Nadal**[1, 2]

[1] Laboratoire de Physique Statistique, École Normale Supérieure, PSL University, Université Paris Diderot, Université Sorbonne Paris Cité, Sorbonne Université, CNRS, 75005 Paris, France.
[2] Centre d'Analyse et de Mathématique Sociales, École des Hautes Études en Sciences Sociales, PSL University, CNRS, 75006 Paris, France.

Corresponding author: Kevin Berlemont. Postal address: Laboratoire de Physique Statistique, ENS, 24 rue Lhomond, 75231 Paris cedex 05, France. Email: kevin.berlemont@lps.ens.fr

Abstract Perceptual decision-making is the subject of many experimental and theoretical studies. Whereas most modeling analyses are based on statistical processes of accumulation of evidence, less attention is being devoted to the modeling with attractor network dynamics, even though they describe psychophysical and neurophysiological data well. In particular, very few works confront attractor models' predictions with data from continuous sequences of trials.

Recently however, numerical simulations of a biophysical competitive attractor network model have shown that such network can describe sequences of decision trials and reproduce repetition biases observed in perceptual decision experiments. Here we get more insights into such effects by considering an extension of the reduced attractor network model of Wong and Wang (2006), taking into account an inhibitory current delivered to the network once a decision has been made. We make explicit the conditions on this inhibitory input for which the network can perform a succession of trials, without being either trapped in the first reached attractor, or losing all memory of the past dynamics. We study in details the reaction times and accuracy properties during a sequence of decision trials. Here we show that, quite remarkably, *in the absence of any feedback* about the correctness of the decision, the network exhibits, qualitatively and with the correct orders of magnitude, post-error slowing and post-error improvement in accuracy, two subtle effects observed in behavioral experiments. Our work thus provides evidence that such effects result from intrinsic properties of the nonlinear neural dynamics.

Significance statement

Much experimental and theoretical work is being devoted to the understanding of the neural correlates of perceptual decision making. In a typical behavioral experiment, animals or humans perform a continuous series of binary discrimination tasks. To model such experiments, we consider a biophysical decision-making attractor neural network, taking into account an inhibitory current delivered to the network once a decision is made. Here we provide evidence that the same intrinsic properties of the nonlinear network dynamics underpins various sequential effects reported in experiments. Quite remarkably, in the absence of feedback on the correctness of the decisions, the network exhibits post-error slowing (longer reaction times after error trials) and post-error improvement in accuracy (smaller error rates after error trials).

Introduction

Typical experiments on perceptual decision-making consist of series of successive trials separated by a short time interval, in which performance in identification and reaction times are measured. The most studied protocol is the one of Two-Alternative Forced-Choice (TAFC) Task – see e.g. Ratcliff (1978); Laming (1979b); Vickers (1979); Townsend and Ashby (1983); Busemayer and Townsend (1993); Shadlen and Newsome (1996); Usher and McClelland (2001); Ratcliff (2004). Several studies have demonstrated strong serial dependence in perceptual decisions between temporally close stimuli (Fecteau and Munoz, 2003; Jentzsch and Dudschig, 2009; Danielmeier and Ullsperger, 2011). Such effects have been studied in the framework of statistical models

of accumulation of evidence (Dutilh et al., 2011), the most common theoretical approach to perceptual decision-making, see e.g. Ratcliff (1978); Ashby (1983); Shadlen et al. (2006); Ratcliff and McKoon (2008); Bogacz (2009), or with a more complex attractor network with additional memory units specifically implementing a biasing mechanism (Gao et al., 2009).

Wang (2002) proposed an alternative approach to the modeling of perceptual decision making based on a biophysical cortical network model of leaky integrate-and-fire (LIF) neurons. The model is shown to account for random dot experiments results of Shadlen and Newsome (2001); Roitman and Shadlen (2002). This decision-making attractor network has been first studied in the context of a task requiring to keep in memory the last decision. This working memory effect is precisely achieved by having the network activity trapped into an attractor state. However, in the context of consecutive trials, the neural activities have to be reset in a low activity state before the onset of the next stimulus. Bonaiuto et al. (2016) have considered a parameter range of weaker excitation where the working memory phase is suppressed. The main result is that the performance of the network is biased towards the previous decision, an effect which decreases with the inter-trial time. Due to the slow relaxation dynamics in the model, the authors only study inter-trial times longer than 1.5 s. However, sequential effects have been reported for shorter inter-trial times, such as 500 ms in Laming (1979b); Danielmeier and Ullsperger (2011).

Instead of decreasing the recurrent excitation, an alternative is to introduce an additional inhibitory input following a decision (Lo and Wang, 2006; Engel et al., 2015; Bliss and D'Esposito, 2017). Lo and Wang (2006) have proposed such a mechanism to account for the control of the decision threshold. However, they do not study the model behavior in the context of sequential trials.

The purpose of the present paper is to revisit this issue of dealing with sequences of successive trials within the framework of attractor networks as introduced by Wang (2002), with a focus on inter-trial times as short as 500 ms. We do so by taking advantage of the reduced model of Wong and Wang (2006) which is amenable to mathematical analysis. This model consists of an effective network of two units, representing the pool activities of two populations of cells, each one being specific to one of the two stimulus categories. Wong and Wang (2006) derive the equations of the reduced model. They choose the parameters values in order to preserve as much as possible the dynamical and behavioral properties of the original full model. In line with Lo and Wang (2006), we take into account an inhibitory current originating from the basal ganglia, occurring once a decision has been made. We explore the serial dependence effects predicted by the model and compare with empirical findings such as sequential bias in decisions (Soetens et al., 1985; Cho et al., 2002). Our main finding is that, without any fine tuning of parameters, the model reproduces two main post-error adjustments in the absence of feedback on the correctness of the decision: post-error slowing (PES) and post-error improvement in accuracy (PIA), PES consisting of longer reaction times, and PIA of smaller error rates, for trials following a trial with incorrect decision.

Materials and Methods

We are interested in modeling experiments where a subject has to decide whether a stimulus belongs to one or the other of two categories, hereafter denoted L and R. A specific example is the one of random dot experiments (Shadlen and Newsome, 2001; Roitman and Shadlen, 2002), where a monkey performs a motion discrimination task in which it has to decide whether a motion direction, embedded into a random dot motion, is towards left (L) or right (R). We consider a decision-making recurrent network of spiking neurons governed by local excitation and feedback inhibition, as introduced and studied in Compte et al. (2000) and Wang (2002). Since mathematical analysis is harder to be performed for such complex networks, without a high level of abstraction (Miller and Katz, 2013), one must rely on simulations which, themselves, can be computationally heavy. For our analysis, we make use of the reduced firing-rate model of Wong and Wang (2006) obtained by a systematic reduction of the detailed biophysical attractor network model. The reduction aimed at faithfully reproducing not only the behavioral behavior of the full model, but also the firing rate dynamics and the output synaptic gating variables. This is done within a mean-field approach, with calibrated simplified F-I curves for the neural units, and in the limit of slow NMDA gating variables motivated by neurophysiological data. The full details can be found in Wong and Wang (2006) (main text and Supplementary Information).

Since this model has been built to reproduce as faithfully as possible the neural activity of the full spiking neural network, it can be used as a proxy for simulating the full spiking network (Engel and Wang, 2011; Deco et al., 2013; Engel et al., 2015). Here, we also make use of this model to gain better insights into the

understanding of the model behavior. In particular, one can conveniently represent the network dynamics in a 2-d phase plane and analyze the network dynamics (Wong and Wang, 2006).

A reduced recurrent network model for decision-making.

We consider the model architecture illustrated in Fig. 1. We first present the architecture without the corollary discharge (Wong and Wang (2006), Fig. 1-1 panel A), which consists of two competing units, each one representing an excitatory neuronal pool, selective to one of the two categories, L or R. The two units inhibit one another, while they are subject to self-excitation. The dynamics is described by a set of coupled equations for the synaptic activities S_L and S_R of the two units L and R:

$$i \in \{L, R\}, \quad \frac{\mathrm{d}S_i}{\mathrm{d}t} = -\frac{S_i}{\tau_S} + (1 - S_i)\,\gamma f\,(I_{i,tot}) \tag{1}$$

The synaptic drive S_i for pool $i \in \{L, R\}$ corresponds to the fraction of activated NMDA conductance, and $I_{i,tot}$ is the total synaptic input current to unit i. The function f is the effective single-cell input-output relation (Abbott and Chance, 2005), giving the firing rate as a function of the input current:

$$f\,(I_{i,tot}) = \frac{aI_{i,tot} - b}{1 - \exp\left[-d\,(aI_{i,tot} - b)\right]} \tag{2}$$

where a, b, d are parameters whose values are obtained through numerical fit.

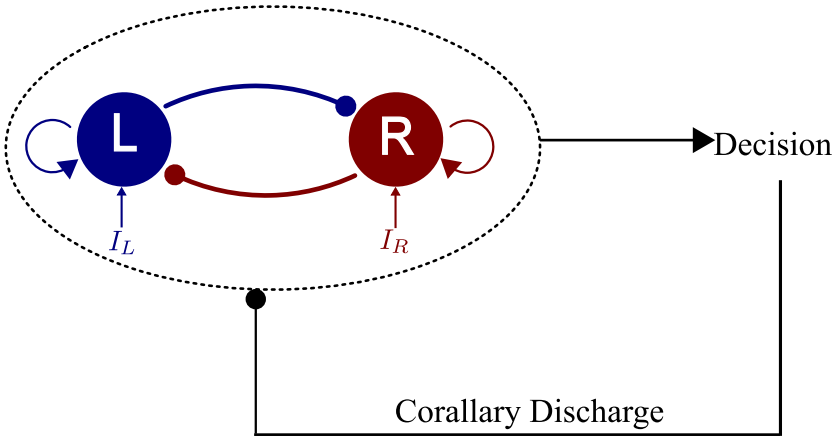

Figure 1: **Architecture of the extended two-variables model.** *Reduced two-variable model constituted of two neural units, endowed with self-excitation and effective mutual inhibition. The extension consists of the addition of the corollary discharge originating from the basal ganglia, an inhibitory input onto both units occurring just after a decision is made.*

The total synaptic input currents, taking into account the inhibition between populations, the self-excitation, the background current and the stimulus-selective current can be written as:

$$I_{L,tot} = J_{L,L}S_L - J_{L,R}S_R + I_{stim,L} + I_{noise,L} \tag{3}$$
$$I_{R,tot} = J_{R,R}S_R - J_{R,L}S_L + I_{stim,R} + I_{noise,R} \tag{4}$$

with $J_{i,j}$ the synaptic couplings. The minus signs in the equations make explicit the fact that the inter-units connections are inhibitory (the synaptic parameters $J_{i,j}$ being thus positive or null). The term $I_{stim,i}$ is the stimulus-selective external input. If μ_0 denotes the strength of the signal, the form of this stimulus-selective current is:

$$I_{stim,i} = J_{A,ext}\mu_0\,(1 \pm c) \tag{5}$$

with $i = L, R$. The sign, $\pm$, is positive when the stimulus favors population L, negative in the other case. The quantity c, between 0 and 1, gives the strength of the signal bias. It quantifies the coherence level of the

stimulus. In the random dot motion framework, it corresponds to the fraction of dots contributing to the coherent motion. Following Wang (2002), this input forms the pooling of the activities of middle temporal neurons firing according to their preferred directions. This input current is only present during the presentation of the stimulus and is shut down once the decision is made.

In addition to the stimulus-selective part, each unit receives individually an extra noisy input, fluctuating around the mean effective external input I_0:

$$\tau_{noise}\frac{\mathrm{d}I_{noise,i}}{\mathrm{d}t} = -\left(I_{noise,i}(t) - I_0\right) + \eta_i(t)\sqrt{\tau_{noise}}\sigma_{noise} \tag{6}$$

with τ_{noise} a synaptic time constant which filter the white-noise. For the simulations, unless otherwise stated parameters values will be those of Table 1.

Parameter	**Value**	**Parameter**	**Value**
a	270 Hz/nA	σ_{noise}	0.02 nA
b	108 Hz	τ_{noise}	2 mS
d	0.154 s	I_0	0.3255 nA
γ	0.641	μ_0	30 Hz
τ_S	100 ms	$J_{A,ext}$	5.2×10^{-4} nA. Hz^{-1}
$J_{N,LL} = J_{N,RR}$	0.2609 nA	$J_{N,LR} = J_{N,RL}$	0.0497 nA
θ	20 Hz		
$I_{CD,max}$	0.035 nA	τ_{CD}	200 ms

Table 1: Numerical values of the model parameters: above the dashed line, as taken from Wong and Wang (2006); below the dashed line, values of the additional parameters specific to the present model (see text).

Initially the system is in a symmetric state, with low firing rates and synaptic activities (see Figure 1-1 panel B). On the presentation of the stimulus, the system evolves towards one of the attractor states, corresponding to the decision state. In these attractors, the 'winning' unit fires at a higher rate than the other. We are interested in reaction time experiments. In our simulations, we consider that the system has made a decision when for the first time the firing rate of one of the two units crosses a threshold θ, fixed here at 20 Hz. We have chosen this parameter value, slightly different from the one in Wong and Wang (2006), from the calibration of the extended model discussed below on sequential decision trials with short response-stimulus intervals. We have checked that this does not affect the psychometric function of the network (see Figure 1-2).

Extended reduced model: inhibitory corollary discharge

Studies (Roitman and Shadlen, 2002; Ganguli et al., 2008) show that, during decision tasks, neurons activity experiences a rapid decay following the responses - see e.g. Figures 7 and 9 in Roitman and Shadlen (2002). Model simulations shows that even when the stimulus is withdrawn at the time of decision, the decrease in activity is not sufficiently strong to account for the empirical findings (see Extended Figure 1-3). Decreasing the recurrent excitatory weights does allow for a stronger decrease in activity, as shown by Bonaiuto et al. (2016). However, both the increase and the decay of activities are too slow, and the network cannot perfom sequential decisions with RSIs below 1sec (see Extended Figure 1-3). Hence the decrease in activity requires an inhibitory input at the time of the decision.

Such inhibitory mechanism has been proposed to originate from the superior colliculus (SC), controlling saccadic eye movements, and the basal ganglia-thalamic circuit (BG), which plays a fundamental role in many cognitive functions including perceptual decision-making. Indeed, the burst neurons of the SC receive inputs from the parietal cortex and project to midbrain neurons responsible for the generation of saccadic eye movements (Hall and Moschovakis, 2003; Scudder et al., 2002). Thus the threshold crossing of the cortical neural activity is believed to be detected by the SC (Saito and Isa, 2003). In turn, the SC projects feedback connections on cortical neurons (Crapse and Sommer, 2009). At the time of a saccade, SC neurons emit a corollary discharge (CD) through these feedback connections (Sommer and Wurtz, 2008). The impact of this CD as an inhibition has been discussed in various contexts (Crapse and Sommer, 2008; Sommer and Wurtz, 2008; Yang

et al., 2008). The generation of a corollary discharge resulting in an inhibitory input has been proposed and discussed in several modelling works, in the case of the modulation of the decision threshold in reaction time tasks (Lo and Wang, 2006), in the context of learning (Engel et al., 2015), and in a ring model of visual working memory (Bliss and D'Esposito, 2017). We note here that, for simplicity and in accordance with the existing literature (Lo and Wang, 2006; Engel et al., 2015; Bliss and D'Esposito, 2017), we will be referring to the inhibitory current resulting from the corollary discharge as the *corollary discharge*.

In the context of attractor networks for decision tasks, Lo and Wang (2006) introduce an extension of the biophysical model of Wang (2002) consisting in modeling the coupling between the network, the basal ganglia and the superior colliculus. The net effect is an inhibition onto the populations in charge of making the decision. While Lo and Wang (2006) address the issue of the control of the decision threshold, they do not discuss the relaxation dynamics induced by the corollary discharge, nor the effects on sequential decision tasks.

In order to analyze these effects with the reduced attractor network model, we assume that, after crossing the threshold, the network receives an inhibitory current, mimicking the joint effect of basal-ganglia and superior colliculus on the two neural populations (Figure 1). In the case of Engel et al. (2015), the function of the corollary discharge is to reset the neural activity in order to allow the network to learn during the next trial. For this, the form of the CD input is chosen as a constant inhibitory current during a period of 300ms. However, such strong input leads to an abrupt reset to the neural state with no memory of the previous trial. We thus rather consider here a smooth version of this discharge, considering that the resulting inhibitory input has a standard exponential form (Finkel and Redman, 1983). The inhibitory input, $I_{CD}(t)$, is then given by:

$$I_{CD}(t) = \begin{cases} 0 & \text{during stimulus presentation} \\ -I_{CD,max} \exp\left(-(t - t_D)/\tau_{CD}\right) & \text{after the decision time, } t_D \end{cases} \tag{7}$$

The relaxation time constant τ_{CD} is chosen in the biological range of synaptic relaxation times and in accordance with the relaxation-times range of the attractor (see Table 1-1), $\tau_{CD} = 200$ ms. Therefore the input currents are modified as follows:

$$I_{L,tot}(t) = J_{LL} S_L(t) - J_{L,R} S_R(t) + I_{stim,L}(t) + I_{noise,L}(t) + I_{CD}(t) \tag{8}$$

$$I_{R,tot}(t) = J_{RR} S_R(t) - J_{R,L} S_L(t) + I_{stim,R}(t) + I_{noise,R}(t) + I_{CD}(t). \tag{9}$$

In Fig. 2 we illustrate the network dynamics between two consecutive stimuli during a sequence of trials, with or without the corollary discharge. In the absence of the CD input, the network is not able to make a new decision different from the previous one (Figure 2.A). Even when the opposite stimulus is presented, the system cannot leave the attractor previously reached, unless in presence of an unrealistic strong input bias. If however the strength $I_{CD,max}$ is strong enough, the corollary discharge makes the system to escape from the previous attractor and to relax towards near the neutral resting state with low firing rates. If too strong, or in case of a too long RSI, at the onset of the next stimulus the neutral state has been reached and memory of past trials is lost. For an intermediate range of parameters, at the onset of the next stimulus the system has escaped from the attractor but is still on a trajectory dependent on the previous trial (Figure 2.B).

With the inhibitory corollary discharge, after the threshold is crossed by one of the two neural populations, there is thus big drop in the neuronal activity (Figure 2.B), corresponding to the exit from the previous attractor state. This type of time-course is in agreement with the experimental findings of Roitman and Shadlen (2002); Ganguli et al. (2008), who measure the activity of LIP neurons during a decision task. They show that neurons that accumulate evidence during decision tasks experience rapid decay, or inhibitory suppression, of activity following responses, similar to Figure 2.B (but see Lo and Wang (2006) for a related modeling study with spiking neurons, or Gao et al. (2009) for rapid decay of neural activity with an other type of attractor network).

During the relaxation period, the amount by which the activities decay determines the initial neural state at the onset of the next stimulus, thus leading to possible biases in the next decision. To understand in more details these phenomena, we represent a bifurcation diagram and an analysis of the phase-plane dynamics in Figure 3. To this end, we need to consider the dynamics after a decision has been made (hence without external excitatory inputs), under two kinds of inhibitory currents: a constant (time-independent) one (Figure 3.A-C-D-G) and the one with an exponential relaxation (Figure 3.B-E-F-H). Fist consider the case of a constant inhibitory input. At small values of the inhibitory current, the attractor landscape is qualitatively unchanged: the dynamics in the absence of noise has three fixed points, one associated with each category and the neutral one (Figure 3.C). At some critical value, of about 0.0215 nA, there is a bifurcation (Figure 3.G): for larger values of the inhibitory

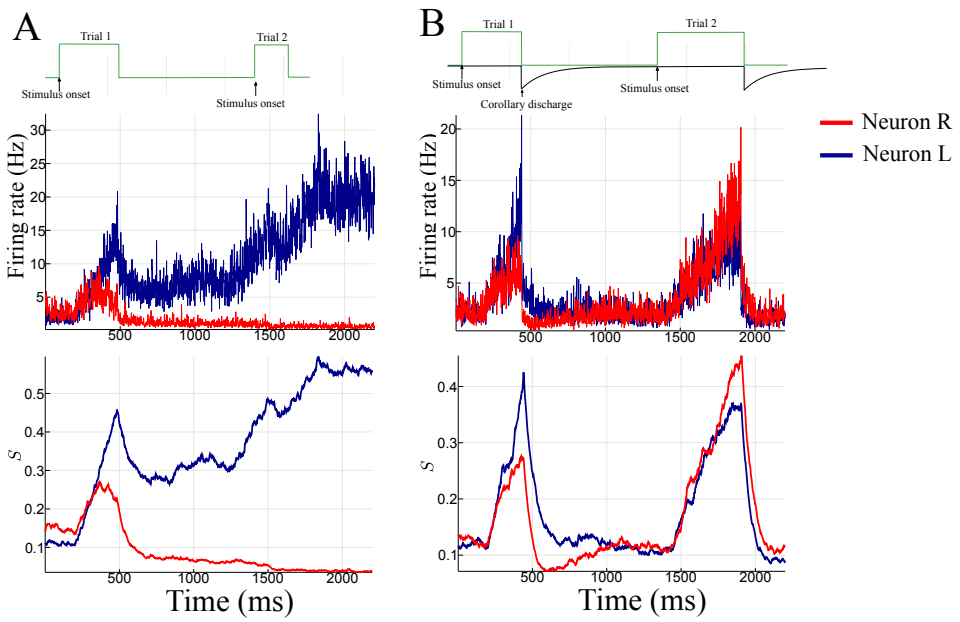

Figure 2: **Time course of activities.** *Activities versus time during two consecutive trials. (A) Simulation without the inhibition due to the corollary discharge. Top (green plot): Time course of the stimulations. The first stimulus belongs to category L, the second to category R. Middle: firing rates of the L (blue) and R (red) neural pools. Bottom: corresponding synaptic activities. The neural activity becomes stuck in the attractor corresponding to the first decision. (B) Simulation with the corollary discharge, with $I_{CD,max} = 0.035$ nA. Top: Time course of the stimulations (green plot, same protocol as for (A)), and time course of the inhibitory current (black curve, represented inverted for clarity of the presentation). Middle and Bottom: neural and synaptic activities, respectively (L: Blue, R: Red). In that case, one observes the decay of activity after a decision has been made, and the winning population is different for the two trials.*

current, the dynamics has only one fixed point, the neutral one (Figure 3.D). As a result, applying a constant CD will either have no effect on the attractor landscape - current amplitude below the critical value -, so that the dynamics remains within the basin of attraction of the attractor reaches at the previous trial; or will reset the activity at the neutral state (current amplitude above the critical value), loosing all memory of the previous decision.

Now in the case of a CD with a value decreasing with time, the network behavior will depend on where the dynamics lie at the time of the onset of the next stimulus. We thus consider the dynamics starting from a decision state (e.g. near the blue attractor in Figure 3.E-F). The networks dynamics is more easily understood by considering the limit of slow relaxation (large time constant τ_{CD}). Between times t and $t + \Delta t$, with Δt small compared to τ, the dynamics is similar to what it would be with a constant CD with amplitude $I_{CD}(t)$. Hence if $I_{CD}(t)$ is larger than the critical value discussed above, the dynamics 'sees' a unique attractor, the neutral state, and is driven towards it. When $I_{CD}(t)$ becomes smaller than the critical value, the system 'sees' again three attractors, and finds itself within the basin of attraction of either the initial fixed point (corresponding to the previous decision, Figure 3.E), or of the neutral fixed point (Figure 3.F). In the later case, the network is able to engage in a new decision task. Sequential effects will exists if, however, at the time of the onset of the new stimulus, the system is still close from the basin boundary.

To conclude, to have the network performing sequential decision tasks, one needs $I_{CD,max}$ to be larger than the critical value (about $I_{CD} = 0.0215$ nA, Figure 2.B), and, for a given value of $I_{CD,max}$, to have a time constant τ_{CD} large enough compared to the RSI for the system to relax close enough to the neutral attractor at the onset of the next stimulus. However, sequential effects will exists only if the current decreases sufficiently rapidly.

Numerical simulations design and Statistical tests

Numerical simulations

In Figure 4 we give a schematic representation of a simulation of sequential decision-making. Each orange rectangle corresponds to a stimulus, with a random value of coherence in the desired range. The stimulus is present until a decision is made. The set of dynamical equations (1,6) – with the definitions (2,5,7,8,9) – is integrated using Euler-Maruyama method with a time step of 0.5 ms. At the beginning of a simulation, the system is set in a symmetric state $S_L = S_R = s_0$, with low firing rates and synaptic activities, $s_0 = 0.1$. We compute the instantaneous population firing rates, or the synaptic dynamical variables S_L and S_R, by averaging on a time window of 2 ms, slided with a time step of 1 ms. The accuracy of the network's performance is defined as the percentage of trials in which the units crossing the threshold corresponds to the stronger input. For data analysis we mainly work with the variables S_L and S_R which are analog to the firing rates R_L and R_R but are less noisy (see Fig 2). We consider that the system has made a decision when for the first time the firing rate of one unit crosses a threshold θ, fixed at 20 Hz. The reaction time during one trial is defined as the time needed for the network to reach the threshold from the start of the input stimulus. We neglect the possible additional time due to motor reaction.

We list in Table 1 the model parameters which correspond to the one of the simulations. For Figures 5 and 7 we have used continuous sequences of 1000 trials averaged over 24 independent simulations (in order to compare with experiments of Bonaiuto et al. (2016) done with 24 subjects). Figures 9 to 16 present results obtained for sequences of 1000 trials averaged over 50 independent simulations.

Statistical tests

Following Benjamin et al. (2018), we consider a p-value of 0.005 as a criterion for rejecting the null hypothesis in a statistical test. To assess if the distributions of two continuous variables are different, we make use of the Kolmogorov-Smirnov test (Hollander et al., 2014), and in the case of discrete distributions we use the Anderson-Darling test (Shorack and Wellner, 2009). For very large samples, we use the energy distance (Rizzo and Székely, 2016), which is a metric distance between the distributions of random vectors. We use the associated E-statistic (Szekely and Rizzo, 2013) for testing the null hypothesis that two random variables X and Y have the same cumulative distribution functions. For testing whether the means of two samples are different we make use of the Unequal Variance test (Welch's test) (Hollander et al., 2014).

Softwares and Code accessibility

For the simulations we made use of the Julia language (Bezanson et al., 2014). The code of the simulations

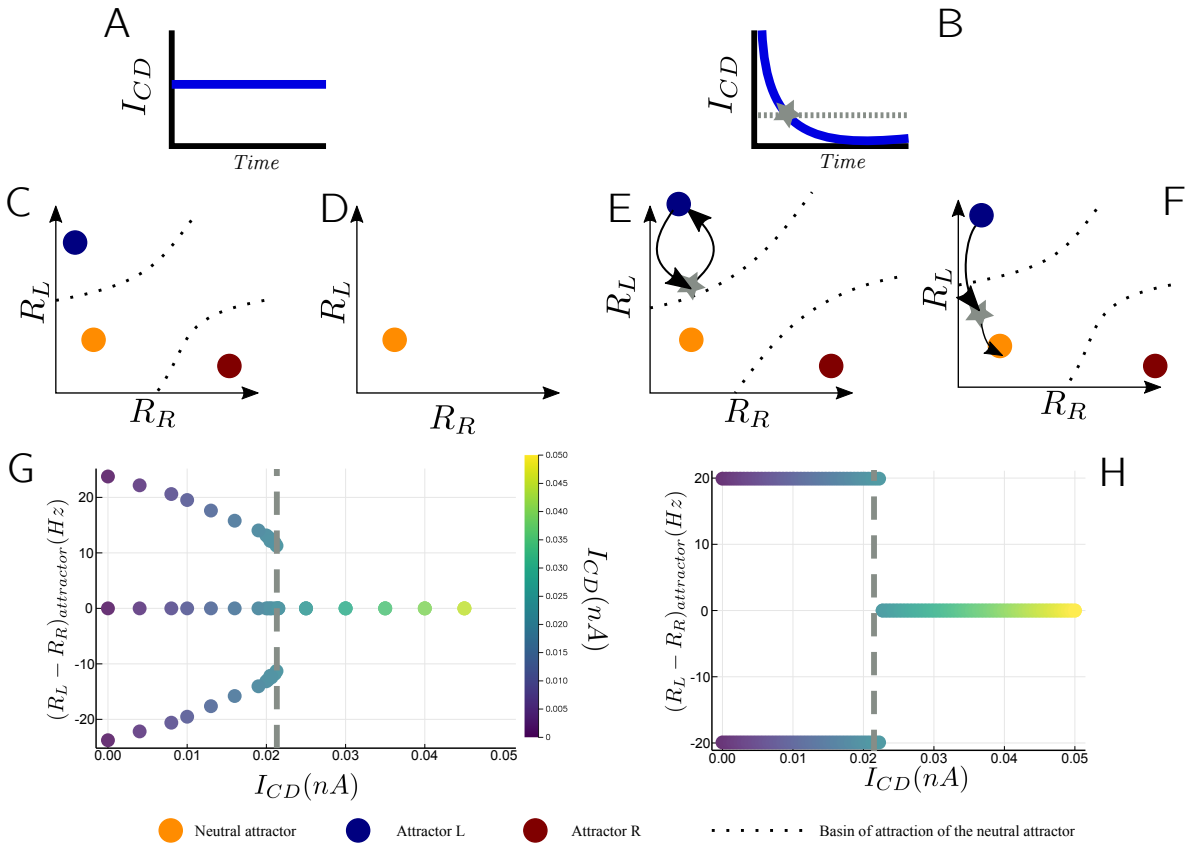

Figure 3: **Bifurcation diagram of sequential decision making.** *(A) Scenario with a constant value of the inhibitory current for the left part of the figure, panels C, D and G. (B) Scenario with an inhibitory current decreasing exponentially with time, for the right part of the figure, panels E, F and H. The dashed line corresponds to $I_{CD} = 0.0215$ nA, value at which the bifurcation at constant I_{CD} occurs (see panel G). The time at which the current amplitude crosses this value is denoted by the gray star in panels E and F. (C) Phase plane representation of the attractors at low I_{CD} (below the critical value). (D) Phase plane representation of the attractor landscape at high I_{CD} (above the critical value). Only the neutral attractor exists, corresponding to the right side of panel G. (E) Schematic phase-plan dynamics corresponding to the left side of (H). The blue attractor corresponds to the starting point and the black arrow represents the dynamics. At the time I_{CD} becomes lower than 0.0215 nA (gray star), the system is still within the basin of attraction of the initial attractor. Hence, it goes back to the initial attractor. (F) Schematic phase-plan dynamics corresponding to the right side of panel H. At the time I_{CD} becomes lower than 0.0215 nA, the system lies within the basin of attraction of the neutral attractor. Hence, the dynamics continues towards the neutral attractor. Those conditions are the ones needed for sequential decision-making. (G) Attractors state (as the difference in firing rates, $R_L - R_R$) with respect to I_{CD}. The gray line, at $I_{CD} = 0.0215$ nA, represents the bifurcation point. On the left side three attractors exists, on the right side only the neutral one exists. The case without inhibitory current corresponds to $I_{CD} = 0$ nA. (H) Attractors that can be reached when starting from a decision state, for the relaxation dynamics under the scenario represented on panel B. On the left side of the dashed gray line, the value of $I_{CD,max}$ is too weak and the network remains locked to the attractor corresponding to the previous decision state. On the right side the network dynamics lies within the basin of attraction of the neutral attractor, allowing the network to engage in a new decision task.*

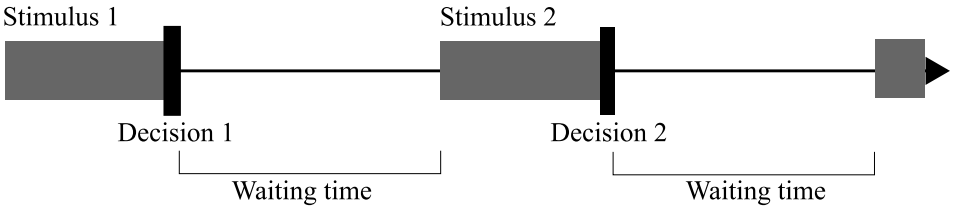

Figure 4: **Simulations protocol.** *The time-sketch of the simulations can be decomposed into a succession of identical blocks. Each block, corresponding to one trial, consists of: the presentation of a stimulus with a randomly chosen coherence (gray box), a decision immediately followed by the removal of the stimulus, a waiting time of constant duration corresponding to the RSI.*

can be obtained from the corresponding author upon request. We made use of the XPP software (Ermentrout and Mahajan, 2003) for the phase-space analysis and the computation of the relaxation time constant of the dynamical system. Figures $8, 9, 10, 11$ and 15 were realized using Python and the other are in the same language as the simulations. The E-statistics tests were performed using the R-Package: *energy package* (Rizzo and Székely, 2014).

Results

Sequential dynamics and choice repetition biases

The qualitative dynamical properties described above, namely the two populations neural dynamics before a decision, followed by the relaxation after decision before the onset of the next stimulus, provide the internal dynamical properties at the origin of sequential effects. This mechanism is described in Bonaiuto et al. (2016) for the analysis of sequence repetition biases. In the present model, although the mechanism is qualitatively the same, the relaxation is induced by the corollary discharge. This results in different quantitative properties, notably in the time scale of the relaxation, which is here more in agreement with experimental findings.
We will show that nonlinear effects are at the core of post-error adjustments. As a preliminary step, it is necessary to describe more precisely the inter trial dynamics. We do so by exploring response repetition bias, as studied in Bonaiuto et al. (2016), and confronting with empirical findings.

In all the following, we explore the model properties in function of the two main parameters, the amplitude of the corollary discharge, $I_{CD,max}$, and the duration of the response-stimulus interval (RSI), that is the time between the response of the subject and the presentation of the next stimulus (in our model the time at which the decision threshold is reached).

Network behavior: Reaction times biases

After running simulations of the network dynamics with the protocol of Figure 4, we analyze the effects of response repetition by separating the trials into two groups, the *Repeated* and *Alternated* cases. The repeated (respectively alternated) trials are those for which the decision is identical to (resp. different from) the decision at the previous trial. Note that we do not consider whether the *stimulus* category is repeated or alternated: the analysis is based on whether the *decision* made by the network is identical or different between two consecutive trials (Fleming, 2010; Padoa-Schioppa, 2013). Such analysis is appropriate, since the effects under consideration depend on the levels of activity specific to the previous decision.

We run a simulation of 1000 consecutive trials, each of them with a coherence value (in percent) randomly chosen between 20 values in the range $[-51.2, 51.2]$. We do so for two values of the corollary discharge amplitude, $I_{CD,max} = 0.035$ nA and $I_{CD,max} = 0.08$ nA, with a RSI of 1 s, the other parameters being given on Table 1.

We find that the distribution of coherence values are identical for the two groups, for both values of $I_{CD,max}$(Anderson-Darling test, $p = 0.75$ and $p = 0.84$ respectively). We study the reaction times separately for the two groups, and present the results in Figure 5. In Figure 5.C we represent the so called energy distance (Szekely and Rizzo, 2013; Rizzo and Székely, 2016) between the repeated and alternated reaction times distribution. As we can observe, the distance decreases, hence the sequential effect diminishes, as the corollary discharge amplitude

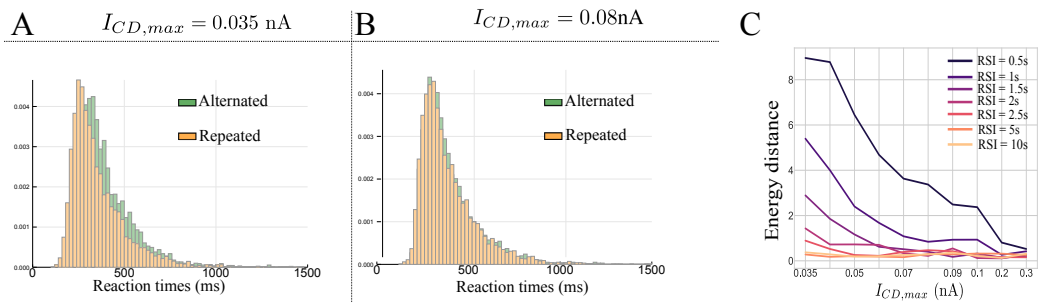

Figure 5: **Histogram of the reaction times.** *We run simulations at (A) $I_{CD,max} = 0.035$ nA and (B) $I_{CD,max} = 0.08$ nA, with a RSI of 1 second. The green histogram corresponds to the Alternated case, that is when the decisions made at the nth and nth $+1$ trials are different. The orange histogram corresponds to the Repeated case, that is when the decisions made at the nth and nth $+1$ trials are identical. (C) Energy distance between the repeated and alternated histograms. The x-axis represents the strength of the corollary discharge, and the color code the duration of the RSI in seconds.*

$I_{CD,max}$ increases. For the specific case of Figures 5.A and B, the corresponding E-statistic for testing equal distributions leads to the conclusion that in the case $I_{CD,max} = 0.035$ nA, the two reaction-time distributions are different ($p = 0.0019$). This implies that the behavior of the network is influenced by the previous trial, and we observe a faster reaction time (around 55 ms) when the choice is repeated (Figure 5A). On the contrary, for $I_{CD,max} = 0.08$ nA (Figure 5.B), the two histograms cannot be distinguished (E-statistic test, $p = 0.25$).

We have checked that increasing the RSI has a similar effect to increasing the corollary discharge amplitude (see Figure 5-1). We observe sequential effects for RSI values in the range 0.5 to 5 seconds, in accordance with psychological experiments, where such effects are observed for RSI less than 5 seconds (Rabbitt and Rodgers, 1977; Laming, 1979b; Soetens et al., 1985; Bonaiuto et al., 2016).

Neural correlates: Dynamics analysis

With the relaxation of the activities induced by the corollary discharge, the state of the network at the onset of the next stimulus lies in-between the attractor state corresponding to the previous decision, and the neutral attractor state. When averaging separately over repeated and alternated trials, we find, as detailed below, that this relaxation dynamics has different behaviors depending on whether the next decision is identical or different from the previous one. Note that this is a statistical effect which can only be seen by averaging over a very large number of trials.

In Figure 6 we compare two examples of network activity, one with an alternated choice, and one with a repeated choice, by plotting the dynamics during two consecutive trials. We observe in Figure 6.A, the alternated case, that previous to the onset of the second stimulus (light blue rectangle) the activities of the two populations are at very similar levels. In contrast, for the case of a repeated choice, Figure 6.C, the activities are well separated, with higher firing rates.

In Figure 6.B we give a classical phase-plane representation of the network dynamics during two consecutive trials, with as axes the synaptic activities of the wining, resp. loosing, populations at the first trial. One sees a trajectory starting from the neutral state, going to the vicinity of the attractor corresponding to the first decision, and then relaxing back to the vicinity of the neutral state; then the trajectory goes to the attractor corresponding to the second decision, different from the first one. This aspect of the dynamics is similar to what is obtained in Gao et al. (2009) with another type of attractor network. We show in Figure 6.D the phase-plane dynamics in the case of a repeated choice (trajectory in blue). On this same panel, for comparison we reproduce in light red the dynamics, shown in Figure 6.B, during the first trial in the alternated case. We observe that the relaxation between trials is different in the two cases. As can be seen in Figure 6.D, the network states at the time of decision are different depending on whether the network makes a decision identical to, or different from, the one made at the previous trial.

In order to check the statistical significance of these observations, we represent in Figure 7 the mean activities during the RSI, obtained by averaging the dynamics over all trials, separately for the alternated and repeated groups. As expected, for small values of $I_{CD,max}$ (0.035 nA), the two dynamics are clearly different. This

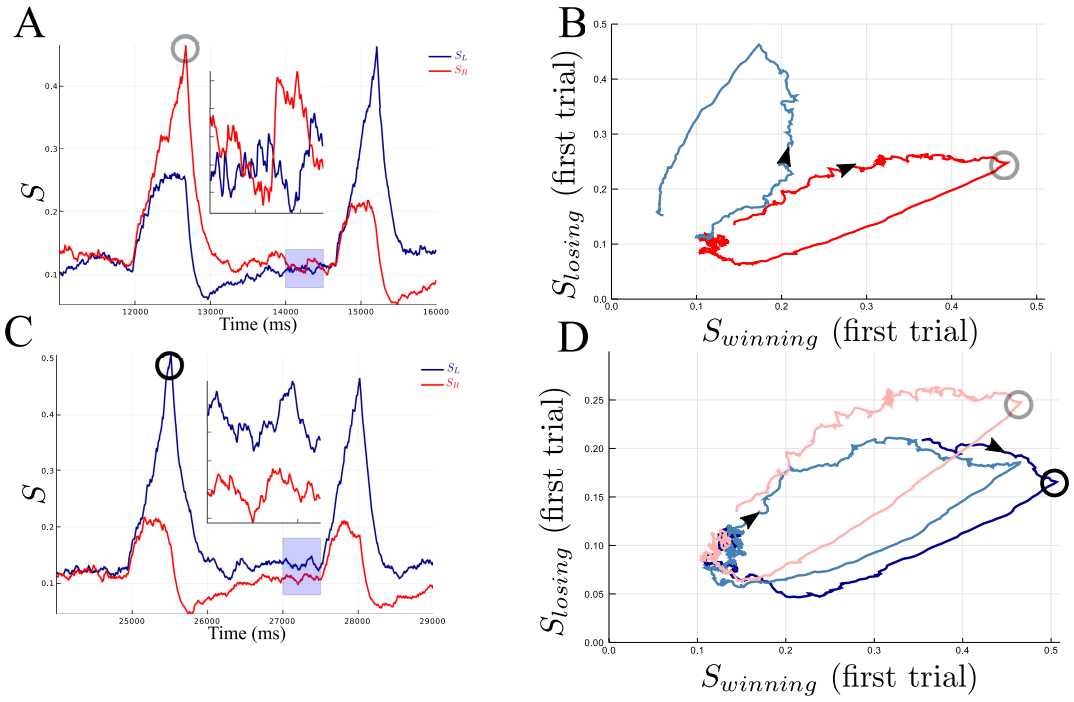

Figure 6: **Network activity during two consecutive trials.** *Panels (A) and (B) represent the alternated case where the decision made is R then L, and panels (C) and (D) represent the case where decision L is made and repeated. Panels (A) and (C) plot the time course activities of the network. The light blue zone is zoomed in order to better see the dynamics just before the onset of the second stimulus. The red and blue curves correspond to the activities of, respectively, the R and L network units. Panels (B) and (D) represent, respectively, the (A) and (C) dynamics in the phase-plane coordinates. On panel (B) the dynamics evolves from dark red (first trial) to light blue (2nd trial), and on panel (D) from dark blue (first trial) toward light blue (2nd trial). The gray – respectively black – circles identify a same specific point during the dynamics in panels (A) and (B) – resp. (C) and (D). The circles are not at the exact same point because the decision threshold is on the firing rates and not for the synaptic activities. In order to compare the alternated and repeated cases, (A,B) and (C, D), the dark red curve of panel (B), is reproduced on panel (D) giving the light red curve.*

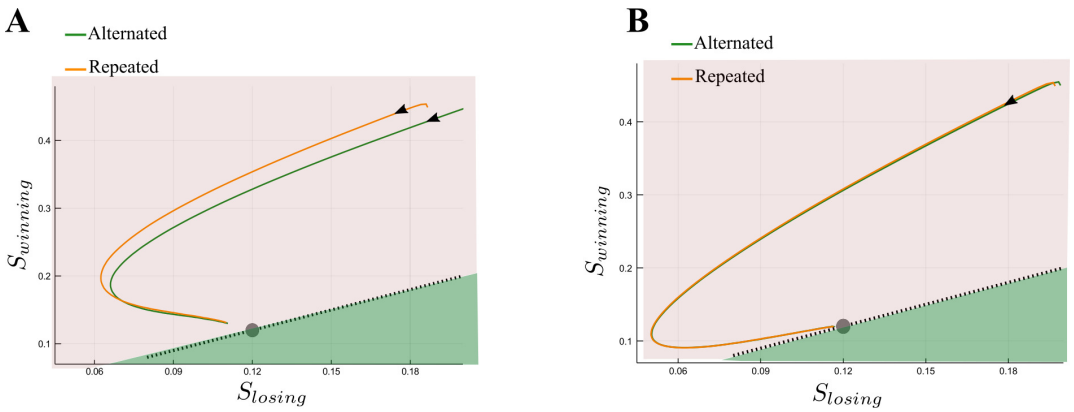

Figure 7: **Phase plane analysis.** *Dynamics of the decaying activity between two successive trials, (A) for $I_{CD,max} = 0.035$ nA, and (B) for $I_{CD,max} = 0.08$ nA. The synaptic activity is averaged over all trials separately for each one of the two groups: alternated (green) and repeated (orange). The axis are $S_{winning}$ and S_{losing} (not S_R and S_L) corresponding to the mean synaptic activity of, respectively, the winning and the losing populations for this trial. Note the difference in scale of the two axes. The time evolution along each curve follows the black arrow. The dashed black line denotes the symmetric states ($S_L = S_R$) of the network, and the gray circle the neutral attractor. The shadow areas represent the basins of attraction (at low coherence levels) for the repeated and alternated trials, respectively pink and green.*

difference diminishes during relaxation. However at the onset of the next stimulus we can still observe some residues, statistically significant according to an Anderson-Darling test done on the 500 ms prior to the next stimulus (between winning population, $p = 0.0034$, between losing population $p = 3.2 \times 10^{-8}$).

These differences in the relaxation dynamics are characteristic of the sequential effects, but they are not the explication of the choice repetition biases. Looking at Figure 7.A, we observe that the ending points of the alternated and repeated relaxations are biased with respect to the symmetric state. At the beginning of the next stimulus the network is already in the basin of attraction of the repeated case. Hence, it will be harder to reach the alternated attractor stated (in the green region). When increasing $I_{CD,max}$ (Figure 7.B), we observe that the ending state of the relaxation is closer to the attractor state. Hence, the biases in sequential effects disappear because at the beginning of the next stimuli the network starts from the symmetric (neutral) state. The same analysis holds for longer RSI (see Figure 7-1), the dynamics are almost identical as can be seen in Figure 7 (Anderson-Darling test: between winning population, $p = 0.25$, between losing population $p = 0.4$), and both relaxation end near the neutral attractor state. The bias depending on the next stimulus is not observed anymore, and the sequential effect on reaction time hence disappears.

The analysis of the dynamics also leads to expectations for what concerns the bias in accuracy towards the previous decision. Indeed, this can be deduced from Figure 7. If the choice at the previous trial was R (respectively L), then, at the end of the relaxation, the network lies closer to the basin of attraction of attractor R (respectively L). Thus when presenting the next stimulus, the decision will be biased towards the previous state, so that the probability of making the same choice will be greater than the one of making the opposite choice. Otherwise stated, given the stimulus presented at the current trial, the probability to make the choice R will be greater when the previous choice was also R, than when the previous choice was L. Numerical simulations confirm this analysis, as illustrated on Figure 7-2. The RSI dependency is statistically significant (Generalized Linear Model: $r = -3.9$, $p < 0.0001$). For small RSI (500 ms), the decision is biased towards the previous one, and for RSI of several seconds this effect disappears. These results are in agreement with experimental findings. Bonaiuto et al. (2016) studied response repetition biases in human with RSIs of at least 1.5 seconds. In these experiments, they measure the Left-Right indecision point, that is the level of coherence resulting in chance selection. Compared to the repeated case, they find that the indecision point for the alternated case is at a higher coherence level, and this shift decreases as the RSI increases.

Sequential decision effects have also been analyzed within the DDM framework (Farrell and Ludwig, 2008; Goldfarb et al., 2012) or with the related LATER model (Kim et al., 2017). Behavioral data can be fitted by different choices of starting points, and possibly of thresholds (Goldfarb et al., 2012). The modification of the starting point in a DDM framework is analog to the effect of the relaxation in our model. However, most works

based on DDM make a post-hoc analysis of empirical data, with separate fits for alternated and repeated cases. In contrast, Kim et al. (2017) consider a global Bayesian approach, in which the starting point corresponds to a prior on the decision, which is updated after each trial to reflect the stimulus history. Such view point implies high order memory effects (see the Discussion section below).

To conclude this section, at the time of decision, the winning population has a firing rate higher than the losing population. After relaxation, at the onset of the next stimulus, the two neural pools have more similar activities, but are still sufficiently different, that is the dynamics is still significantly away from the neutral attractor. At the onset of the next stimulus, the systems finds itself in the basin of attraction of the attractor associated to the same decision as the previous one. This results in a dynamical bias in favor of the previous decision. The probability to make the same choice as the previous one is then larger than the one of the other choice, and the reaction time, for making the same choice (repeated case), is shorter than for making the opposite choice (alternated case). In accordance with these results, studies on the LIP, superior colliculus and basal ganglia have found that the baseline activities before the onset of the stimuli can reflect the probabilities of making the saccade, under specific conditions (Lauwereyns et al., 2002; Ding and Hikosaka, 2006; Rao et al., 2012). Our model shows that these modulations of the baseline activities can be understood as resulting from the across-trials dynamics of the decision process.

Post-error effects

Post-error adjustments on reaction times

The most interesting and well established effect is the one of Post-error slowing (PES) (Laming (1979b)). It consists of prolonged reaction times in trials following an error, compared to reaction times following a correct trial. This effect has been observed in a variety of tasks: categorization (Jentzsch and Dudschig, 2009), flanker (Debener, 2005), Stroop (Gehring and Fencsik, 2001) tasks. Jentzsch and Dudschig (2009) and Danielmeier and Ullsperger (2011) found that the PES effect depends on the response-stimulus interval. The amplitude of this effect, defined as the difference between the mean reaction times, decreases as one increases the RSI, with values going from several dozens of milliseconds to zero. For RSI longer than $750 - 1500$ ms, PES is not observed anymore. Remarkably, the PES effect is reported in cases where the subject does not receive information on the correctness of the decision (Jentzsch and Dudschig, 2009; Danielmeier and Ullsperger, 2011).

In this section we investigate the occurrence of post-error adjustments in our model. We confront the results to empirical findings from experiments where, as it is also the case in our model, there is no feedback on the correctness of the decision. More specifically, we make numerical simulations in order to more easily compare with the findings of Danielmeier and Ullsperger (2011). These authors considered a flanker task with stimuli belonging to one of two opposite categories (Left or Right directions). This protocol thus falls within the class of experiments that our model aims at describing. In the present work we test several coherence levels, each one leading to a different value of the error rate. In the experiments of Danielmeier and Ullsperger (2011), the ambiguity level is not quantified. However, the observed error rates are found around 10% which, within our model, corresponds to a coherence level of about $c = 10\%$. We will thus more specifically discuss this coherence level throughout the section. Finally, in Danielmeier and Ullsperger (2011), each subject performed a total number of 996 trials. In order to make simulations with a similar protocol, we compute the post-error effects for continuous session of 1000 trials.

In Figure 8.A we represent the phase diagram of the PES effect with respect to the coherence level (x-axis) and $I_{CD,max}$ (y-axis), at an intermediate RSI value of 500 ms. We first remark that there are three types of behaviors: post-error slowing effect (PES) (in red) / no effect on the reaction times (in gray) / post-error quickening (PEQ) (in blue). Figure 8.B zooms on a value of $I_{CD,max}$ for which PES occurs ($I_{CD,max} = 0.035$ nA). We observe that the magnitude of the PES effect goes from zero to ten milliseconds, hence remaining within the range of behavioral data (Jentzsch and Dudschig, 2009) (12 ms for a RSI of 1 second). The second remark concerns the variation of the PES effect with respect to the coherence level. In the region where we observe a PES effect, we find that it is enhanced under conditions when errors are infrequent. However, for large values of the coherence level, this effect cannot be observed anymore due to the absence of any error in the successive trials (almost 100% of correct trials). This occurrence of PES, principally at low error rates, has been found in experiments of Notebaert et al. (2009); Núñez Castellar et al. (2010), for which the authors observe PES when errors are infrequent, but not when errors are frequent.

In addition to PES, the model presents a domain in parameter space where reaction times are faster after an error than after a correct trial. We propose to call this effect *post-error quickening* (PEQ), as opposed to

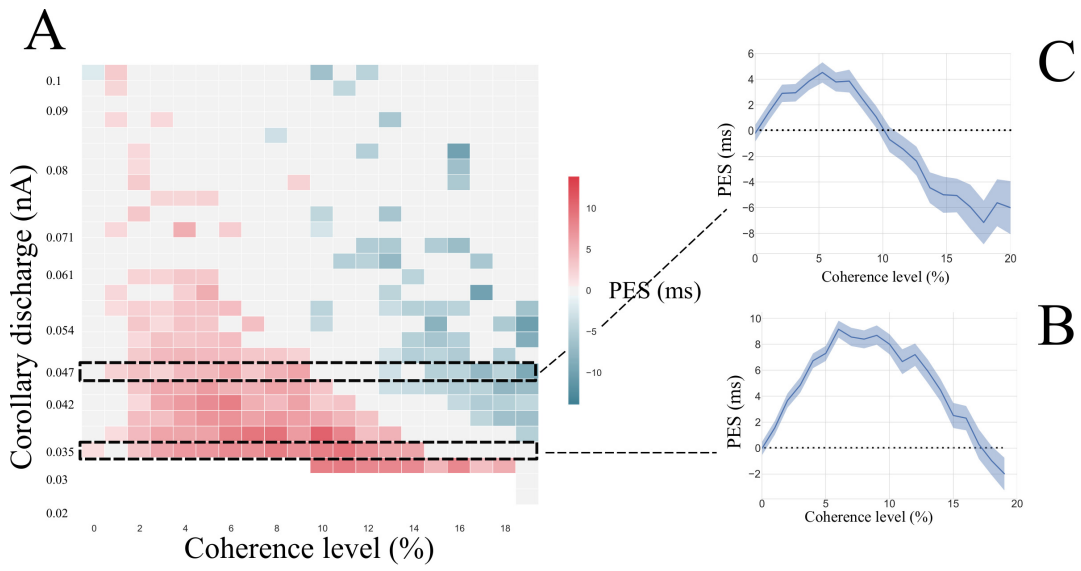

Figure 8: **Post-error slowing in the simulated network at a RSI of 500 ms.** *(A) Phase diagram of the PES effect at RSI of* 500 *ms. The bottom white zone corresponds to parameters where sequential decision-making is impossible as the network is able to leave the attractor state during the RSI . The red square corresponds to regions where PES is observed, and the blue ones where PEQ is observed (the darker the color, the stronger the effect). The black dashed squares correspond to specific regions where Panels B and C zoom. (B) PES effect (ms) with respect to the coherence level at* $I_{CD,max} = 0.035$ *nA. The light blue zone corresponds to the bootstrapped (Efron and Tibshirani, 1994) confidence interval at* 95%*. (C) PES effect (ms) with respect to the coherence level at* $I_{CD,max} = 0.047$ *nA. The light blue zone corresponds to the bootstrapped confidence interval at* 95%*.*

post-error slowing. As shown in Figure 8.C, we find that this effect can occur or not along with PES, depending on the coherence level.

This PEQ effect, although much less studied, has been observed in various experiments (Rabbitt and Rodgers, 1977; Hester et al., 2005; Purcell and Kiani, 2016), notably for fast-response regimes (Notebaert et al., 2009; King et al., 2010). The conditions for observing PEQ remain however not well established, with some contradictory results. For instance, Hester et al. (2005) report post-error decrease in reaction times for aware errors, but not for unaware errors, whereas Cohen (2009) on the contrary reports a larger PES effect for aware errors than for unaware errors. Our model, which exhibits PEQ at high coherence levels, provides predictions (in the absence of feedback) that can be tested. At high coherence, responses are fast. In the rare case of an error, it is more likely for the subject to become aware that an error has been made than in the case of low coherence (high uncertainty on the stimulus category). Hence the fact that PEQ occurs in the model at high coherence levels is more in line with the results of Hester et al. (2005) .

In behavioral experiments the PES effect depends strongly on the RSI. For RSI longer than $1000 - 1500$ ms the observation or not of PES depends specifically on the decision task (Jentzsch and Dudschig, 2009; King et al., 2010). Despite the fact that PES is not always observed for long RSI, a common observation remains: if one keeps increasing the RSI, the PES effect eventually disappears. We investigate this behavior in the context of our network, by plotting the phase diagram at $I_{CD,max} = 0.035$ nA with respect to the RSI (Figure 9).

We observe that, for parameters where PES is observed at 500 ms, increasing the RSI leads to the weakening of the post-error slowing effect until its disappearance. At a RSI of 1600 ms (Figure 9.B) this effect is not present anymore, in agreement with experimental results (Jentzsch and Dudschig, 2009).

Post-error improvement in accuracy

Post-error improvement in accuracy (PIA) is another sequential effect reported in experiments (Laming, 1979b; Marco-Pallarés et al., 2008; Danielmeier and Ullsperger, 2011). PIA has been observed on different timescales: long-term learning effects following error (Hester et al., 2005) and trial-to-trial adjustments directly after

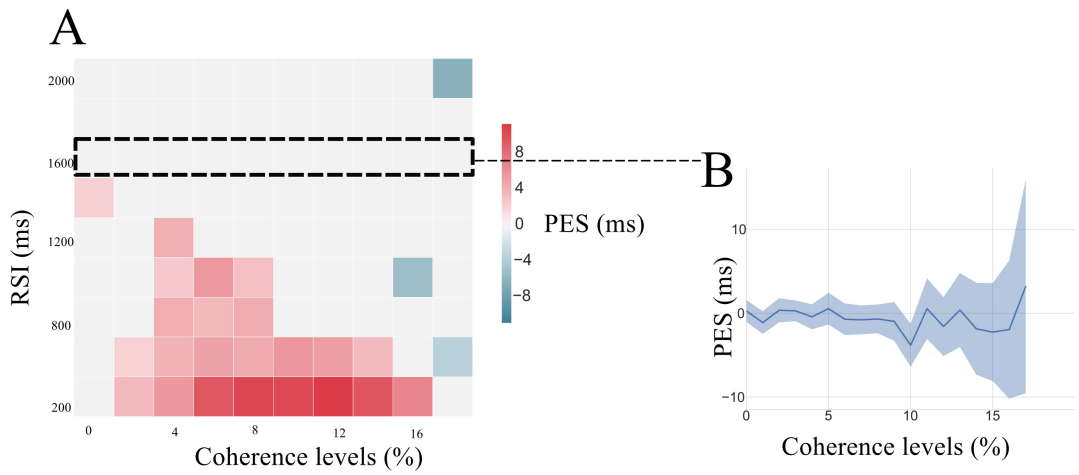

Figure 9: **Post-error slowing depending on RSI.** *(A) Phase diagram of the PES effect at $I_{CD,max} = 0.035$ nA. The red square corresponds to regions where PES is observed (the darker the color, the stronger the effect). The black dashed squares correspond to a specific regions where panel B zooms. (B) PES effect (in ms) with respect to the coherence level at $I_{CD,max} = 0.035$ nA and at RSI of 1600 ms. The light blue zone corresponds to the bootstrapped confidence interval at 95%.*

commission of error responses. We only consider this latter type of PIA. The specific conditions under which PIA can be observed in behavioral experiments have not been totally understood. We investigate this effect in the specific context of our model, the more the difference in accuracy is important the more this effect is considered as important.

In Figure 10 we represent the phase diagram of the PIA effect with respect to coherence levels (x-axis) and corollary discharge amplitude (y-axis). We denote a large region of parameters for which PIA is present. We find a magnitude of the PIA effect of about $2 - 4\%$, which is of the same order of magnitude as in the experiments where, for RSIs in the range $500 - 1000$ ms, it is found that post-error accuracy is improved by approximatively 3% (Jentzsch and Dudschig, 2009).

Looking at Figure 10, one sees that the PIA and PES effects append in the same region of parameters. However, if we zoom in on specific regions (Figure 10.B and C), we can notice some differences in the variation of these effects. The black dashed square regions correspond to the same parameters as in Figure 8. We first note that PIA is also observed in these regions. However, we observe a decrease of PES at very large coherence (Fig. 8.B), but not of PIA (Fig. 10.B). Moreover the decrease of the PIA effect in Figure 8.C does not occur at the same values of parameters as for the PES one.

As stated by Marco-Pallarés et al. (2008), time courses of PES and PIA seem to be dissociable as post-error improvements in accuracy have been observed with longer inter-trial intervals (up to 2250 ms). We investigate the variation with respect to the RSI of PIA in our model (Figure 11). We note that, for long RSIs, the PIA effect is not observed anymore. However as observed in Marco-Pallarés et al. (2008), the PIA effect occurs for longer RSIs than the PES effect (Figure 11.A). In the same way, PIA is more robust with respect to the intensity of the corollary discharge. This is corroborate by the Figure 11-1, which represents PES and PIA effect for $\tau_{CD} = 500$ ms, hence, with a stronger corollary discharge.

Verguts et al. (2011) find that PIA and PES seem to happen independently, suggesting that at least two post-error processes takes place in parallel. An important outcome of our analysis is to suggest that PIA and PES effects both result from the same underlying dynamics.

In addition, in the parameters domain where they both occur, we find that the variations of these effects with respect to the coherence levels are indeed uncorrelated (Pearson correlation test: RSI of 500 ms and $I_{CD} = 0.035$ nA, $p = 0.58$, $I_{CD} = 0.05$, $p = 0.79$ and $I_{CD} = 0.1$ nA, $p = 0.25$; RSI of 2000 ms and $I_{CD} = 0.035$ nA, $p = 0.37$). This non-correlation highlights the complexity of such post-error adjustments, as explored in Verguts et al. (2011).

In order to obtain more insights into the PIA effect, we study the discrimination threshold following an error or a success, with respect to the RSI (Figure 11.C-E). The definition of the *discrimination threshold* is based on the use of a Weibull function commonly used to fit the psychometric curves (Quick, 1974). That is, one writes

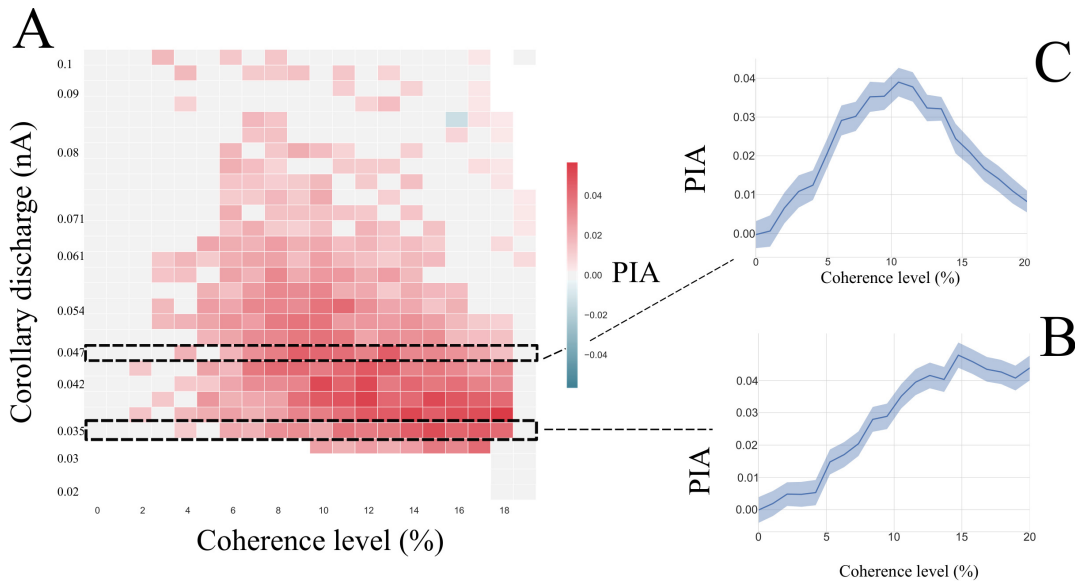

Figure 10: **Post-error improvement in accuracy at a RSI of 500 ms.** *(A) Phase diagram of the PIA effect at RSI of* 500 *ms. The bottom white zone corresponds to parameters where sequential decision-making is impossible. The red square corresponds to regions where PIA is observed. The black dashed squares correspond to specific regions where panels B and C zoom. (B) PIA effect with respect to the coherence level at* $I_{CD,max} = 0.035$ *nA. The light blue zone corresponds to the bootstrapped confidence interval at* 95%*. (C) PIA effect with respect to the coherence level at* $I_{CD,max} = 0.047$ *nA. The light blue zone corresponds to the bootstrapped confidence interval at* 95%*.*

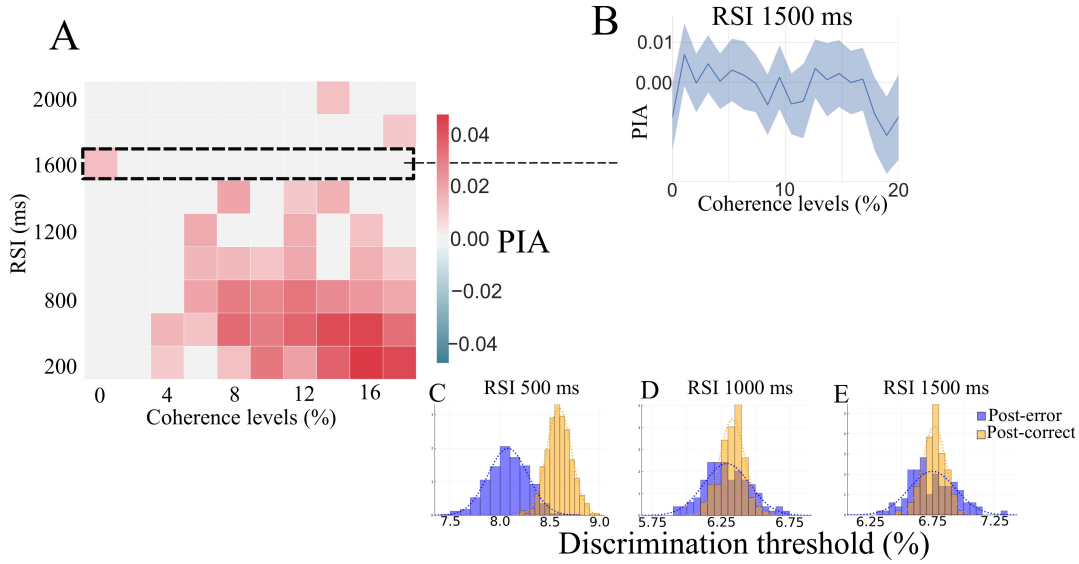

Figure 11: **Post-error improvement in accuracy depending on RSI.** *(A) Phase diagram of the PIA effect at* $I_{CD,max} = 0.035$ *nA. The red square corresponds to regions where PIA is observed. The black dashed squares correspond to specific regions where panels B and C zoom. (B) PIA effect with respect to the coherence level at* $I_{CD,max} = 0.035$ *nA and a RSI of* 1600 *ms. The light blue zone corresponds to the bootstrapped confidence interval at* 95%*. (C)-(D)-(E) Distribution of the discrimination threshold for three values of RSI* $(500, 1000, 1500$ *ms respectively). In yellow we represent the histogram of the post-correct trials, and in blue the post-error ones. The dashed curves of the corresponding color corresponds to the cumulative functions of these distributions. The corollary discharge is* $I_{CD,max} = 0.035$ *nA.*

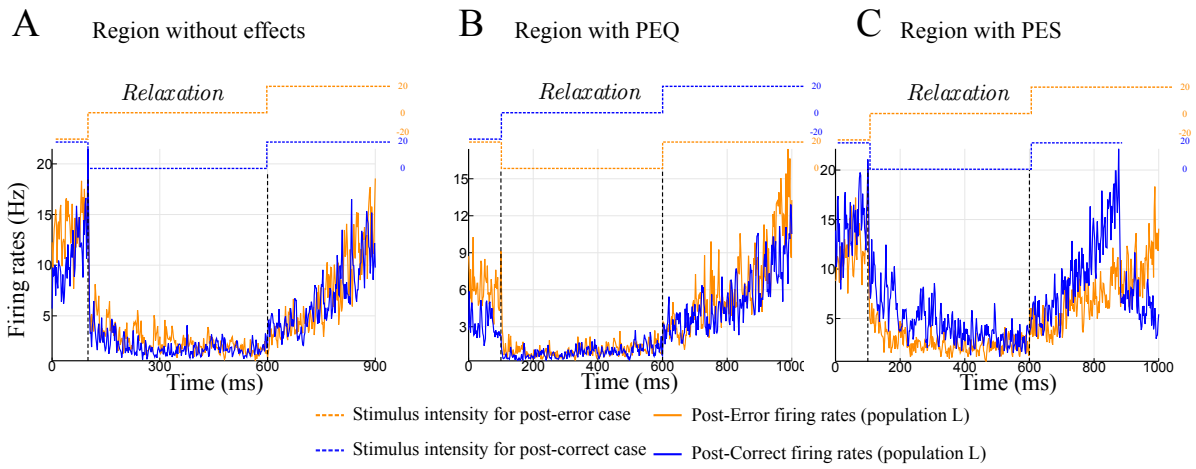

Figure 12: **Neural activities of individual trials.** *(A) Dynamics for individual trials for the winning populations of the next trial: in blue the post-correct case and in orange the post-error one. The dashed lines represent the stimuli with respect to time. The parameters are set to a region without PES or PEQ effects ($I_{CD} = 0.047$ nA and $c = \pm 10\%$). (B) This panel represents the dynamics in the region of PEQ ($I_{CD} = 0.047$ nA and $c = \pm 20\%$). On this trial we can notice that the post-error dynamics is faster than the post-correct one. (C) The parameters are set to the PES region ($I_{CD} = 0.035$ nA and $c = \pm 10\%$). The post-correct dynamics (in blue) reaches the threshold sooner than the post-error one (in orange).*

the performance (mean success rate) as:

$$\text{Perf}(c) = 1 - 0.5 \exp\left(-(c/\alpha)^{\beta}\right) \tag{10}$$

where α and β are parameters. Then, for $c = \alpha$, $\text{Perf}(c) = 1 - 0.5 \exp(-1) \sim 0.82$. Hence one defines the discrimination threshold as the coherence level at which the subject responds correctly 82% of the time.

In Figure 11.C we represent the distribution of the discrimination threshold for $I_{CD,max} = 0.035$ nA and a RSI of 500 ms. For these parameters, the distributions for the post-error and post-success cases are highly different (Smirnov-Kolmogorov test: $p < 10^{-20}$). If we increase the RSI (1000 ms for Figure 11.D and 1500 ms for Figure 11.E), we observe that this difference disappears (Smirnov-Kolmogorov test: $p = 0.038$ and $p = 0.4$ respectively). However, we note that the discrimination threshold distribution is wider after an error than after a correct trial. This might result from the wider distribution in the firing rates (or synaptic activities) after error that we discuss in the next section. To our knowledge, this effect has not yet been studied in human/behavioral experiments.

Dynamical analysis

In this section we analyze the PES and PEQ effects in terms of neural dynamics. First of all, we represent and discuss dynamics on individual trials for the three regions of parameters: with neither PES nor PEQ effects, with PES effect, and with PEQ effect (Figure 12). We observe the dynamics for post-error and post-correct trials during the relaxation period following a decision and during the presentation of the new stimulus. Already on individual trials we notice differences between the regions. Figure 12.A represents a trial in the region without PES or PEQ. The post-error/correct dynamics are indistinguishable. Hence we do not observe any differences in the reaction times. Looking at a trial in the PEQ region (Figure 12.B), we notice that the population L (the winning one for the second stimulus) for the post-error case seems a bit higher in activity than for the post-correct case. This leads to the post-error quickening effect, as the post-error (orange) curve will reach the threshold sooner than the post-correct (blue) one. Finally, Figure 12.C represents individual trials for parameters in the PES region. In the phase diagram the effect was more pronounced than PEQ, thus it is more pronounced on the dynamics too. During the relaxation, and the presentation of the new stimulus, the post-correct dynamics (blue curve) for population L (the winning one for the second stimulus) is higher than the post-error one. As we can observe this leads to a faster decision time for the post-correct trial than for the post-error one.

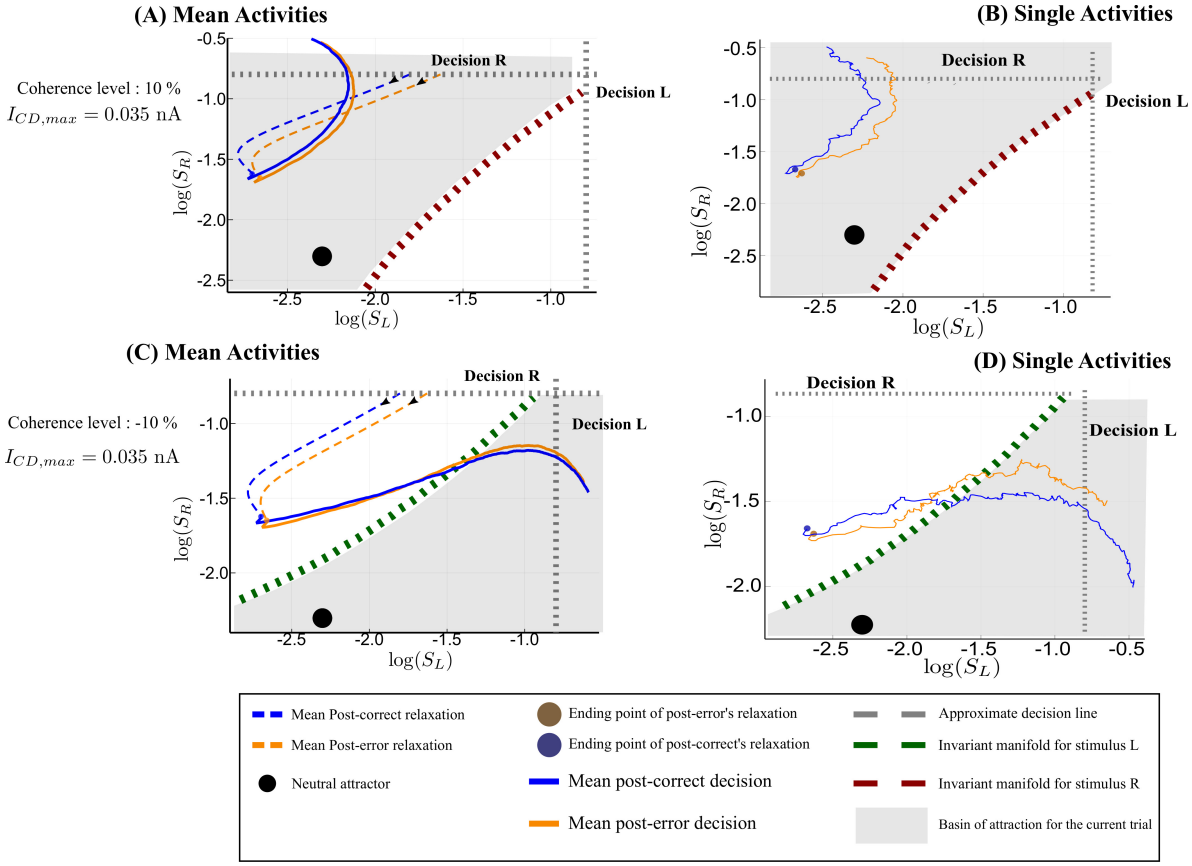

Figure 13: **Analysis of the post-error trajectories for the PES regime.** *Phase-plane trajectories (in log-log plot, for ease of viewing) of the post-correct and post-error trials. We consider that the previous decision was decision R. The black filled circle shows the neutral attractor state (during the relaxation period). During the presentation of the next stimulus, the attractors and basins of attraction change (represented by the gray area and the green or red dashed line). Panels (A) and (B): PES and PIA regime ($c = 10\%$ and $I_{CD,max} = 0.035$ nA) in the repeated case. The blue color codes for post-correct trials, and the orange one for post-error. Panel (A): average dynamics; Panel (B): single trajectories during the next trial. Panels (C) and (D): regime with PES and PIA in the alternated case ($c = -10\%$ and $I_{CD,max} = 0.035$ nA). The dynamics after the relaxation is followed during 400ms for repeated and 800 ms for alternated case, as if there were no decision threshold. The actual decision occurs at the crossing of the dashed gray line, indicating the threshold. This allows to visually compare the associated reaction times.*

We show now that the dynamics explains the three effects PES, PEQ and PIA. We provide in Figures 13 and 14 a semi qualitative and semi quantitative analysis of the dynamics of the synaptic activities in the phase plane of the system, for several parameters regimes. Here again, the analysis is easier working on the synaptic activities. This can be seen by considering Extended Figure 13-1 on which we represent the mean firing rate and synaptic activity of the winning population in the PES case. At the beginning of the next trial, the difference between the post-error and post-correct firing rates is significantly below zero, hence the reaction time will be shorter for post-correct than for post-error trials. The difference in synaptic activities is as well negative, but much less noisy: the effect is thus better seen by working with the synaptic variables.

PES effect. We now detail the analysis of the PES effect (and of the concomitant PIA effect) based on Figures 13. Let us first explain how each panel is done. Without loss of generality, we assume that the last decision made is R. Repeated and Alternated cases thus correspond to next trial decisions R and L, respectively. The x and y axis are the synaptic activities S_L and S_R, respectively – hence, the losing and wining populations for the first trial.

On the left panels, we represent with dashed lines the average dynamics during the relaxation period, that

is from the decision time for the previous stimulus to the onset of the next stimulus. This allows to identify clearly the typical neural states at the end of the relaxation period. The average is done over post-error (resp. post-correct) trajectories sharing a same state at the time of the last decision. The choice of these two initial states is based on the following remark. A typical trial with a correct decision will lead, at the time of decision, to losing and wining populations with highly different activity rates, hence a neural activity, and thus a synaptic activity S_L, far from the threshold value. On the contrary, a typical error trial will show a losing activity not far from the threshold – this can also be observed in Figure 4B in Wong et al. (2007). We can thus represent post-correct trials, respectively post-error trials, by dynamics with initial states having a rather small, respectively large, value of S_L (and in both cases the first trial winning population S_R at threshold value).
We then represent with a continuous line the average trajectory following the onset of the new stimulus. We observe this dynamics during the same time for post-error and post-correct cases, as if there were no decision threshold, in order to compare the dynamics of post-error and post-correct cases for the same duration of time. Decision actually occurs when the trajectory crosses the decision line (dashed gray line) – this, approximately: because of the noise, there is not a one to one correspondence between a neural activity reaching the decision threshold and a particular value of the associated synaptic activity. Having all the trajectories plotted for a same duration (and not only until the decision time) allows to visually compare the associated reaction times.

On the right panels, we represent typical trajectories during the presentation of the new stimulus. The black dot on every panel gives the location of the neutral attractor that exists during the relaxation dynamics. The basins of attractions that are represented are the one associated with the attractors L, R, of the dynamics induced by the onset of the next stimulus. Remind that these attractors are different from the ones associated to the dynamics during the relaxation period.

We can now analyze the dynamics. In the repeated case (Fig. 13.A and B), at the end of the relaxation (that is at the onset of the next stimulus), both post-correct and post-error trials lie into the correct basin of attraction. Hence, the error rates for these trials are similar. However, the neural states reached at the end of the relaxations are different. Compared to the post-error trial, the post-correct state is closer from the boundary of the new attractor associated to decision R, and the corresponding decision will thus be faster. In the alternated case (Fig. 13.C and D), the states reached at the end of the relaxation period do not lie within the correct basin of attraction. During the decision-making dynamics, the trajectory needs to cross the boundary between the two basins of attraction. The post-correct trials leading to an alternate decision have a rather straight dynamics across the boundary, leading to relatively fast decision times. In contrast, the states at the onset of the stimulus of the post-error trials are close enough to the boundary so that the corresponding trajectories crosses with a smaller angle the basin boundary. This leads to longer reaction times, hence the PES effect. However, for specific realizations of the noise that lead to error trials (Fig. 13-2) the post-error trials dynamics is closer to the boundary. Thus it has a higher probability to fall on the other side of the basin of attraction. Hence, the error rates are lower for post-error trials than post-correct trials and that explains the PIA effect.

PEQ effect. The PEQ effect can be understood from the same kind of analysis, based here on Fig. 14 (analogous for the PEQ effect to Fig. 13 for the PES effect). As seen previously, this effect occurs mostly at high level of coherence. We consider first the repeated case (Figure 14.A and B). Since the coherence level is high, at the end of the relaxation period, both post-correct and post-error trials lie within the correct basin of attraction, far from the basin boundary. The reaction times and error rates of post-correct and post-error trials for repeated decisions are thus similar.

In contrast, the alternated case (Fig. 14.C and D) exhibits both the PIA and the PEQ effects. The post-error's end of relaxation now is inside the basin of attraction of the alternated choice. Hence, the error rate will be lower than when the ending point is outside this region (post-correct trials begin at the boundary of the basin of attraction). Moreover, the post-correct trials dynamics have to cross the boundary. Hence they are closer to the manifold, which lead to a slow dynamics, whereas the post-error dynamics can directly reach the new attractor state.

In Figure 14-1.A and B we investigate the parameter regime, at low coherence level, for which there is no effect – neither PES, nor PEQ or PIA. The post-error and post-correct dynamics are very similar and lead to the same relaxation ending point, far from the basin boundary. Finally, in Figure 14-1.C and D we consider the parameter regime, at high coherence level, with only the PIA effect. Here the relaxations of post-error and post-correct trials are different. However, as for the PEQ effect, at high coherence level both dynamics will be fast. For alternated trials, none of the two ending points are in the correct basin of attraction.

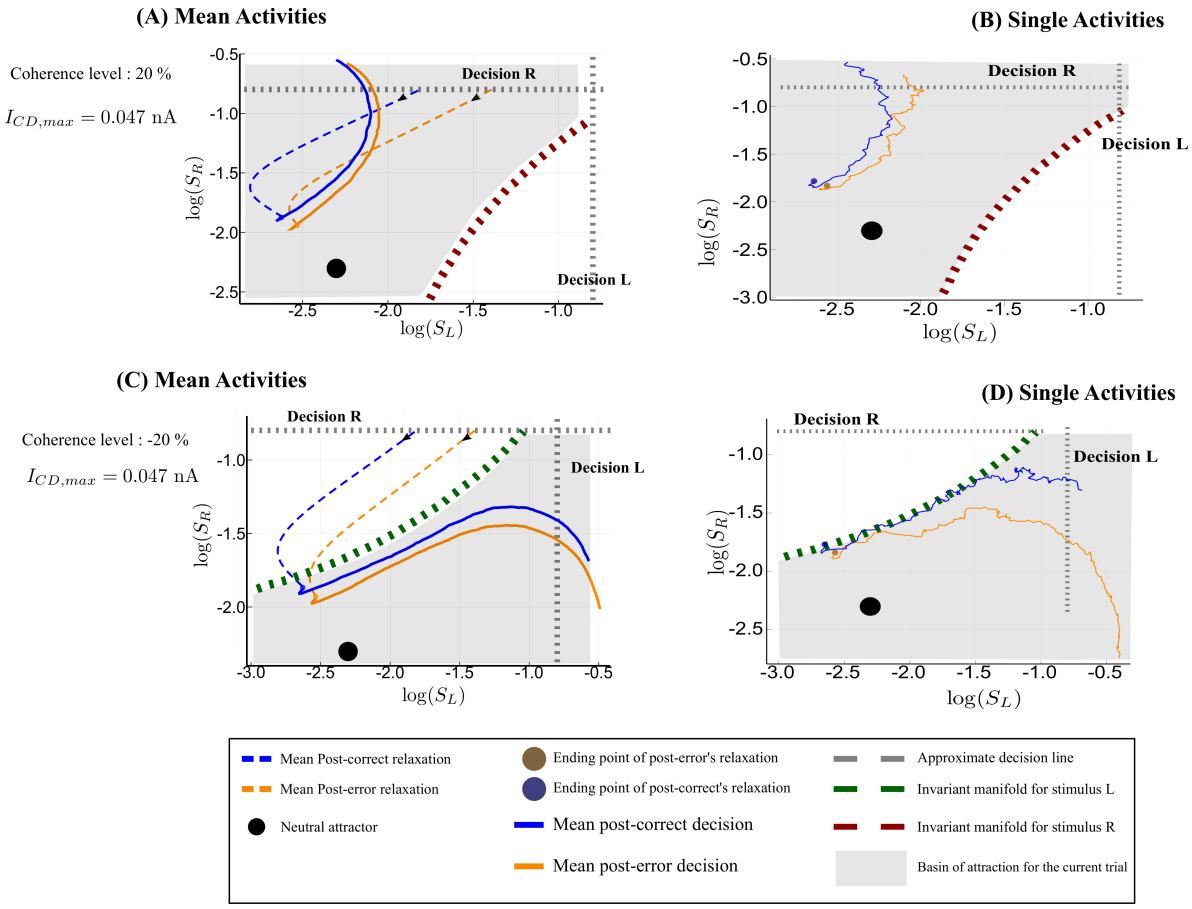

Figure 14: **Analysis of the post-error trajectories in the PEQ regime.** *Phase-plane trajectories (in log-log plot, for ease of viewing) of the post-correct and post-error trials (same as Figure 13 in the PEQ case). We consider that the previous decision was R. The black filled circle shows the neutral attractor state (during the relaxation period). During the presentation of the next stimulus, the attractors and basins of attraction change (represented by the gray area and the green or red dashed line). Panels (A) and (B): PEQ and PIA regime ($c = 20\%$ and $I_{CD,max} = 0.047$ nA). The blue color codes for post-correct trials, and the orange one for post-error. The plain lines represent mean dynamics for (A) or single dynamics (B). Panels (C) and (D): regime with PEQ and PIA in the alternated case ($c = -20\%$ and $I_{CD,max} = 0.047$ nA).The post-error relaxation already lies within the alternated basin of attraction. For alternated trials, the dynamics needs to cross the invariant manifold (green dashed line), which denotes the boundary between the basins of attraction. The dynamics is followed during 400ms for repeated and 800 ms for alternated case, as if there were no decision threshold. The actual decision occurs at the crossing of the dashed gray line, indicating the threshold. This allows to visually compare the associated reaction times.*

Correlating post-error effects with the activity distributions at the previous decision. To go beyond the above analysis on the post-error adjustments, we analyze the respective influence of the winning and losing population levels of activity at the time of the previous decision, onto the decision at the next trial. This will first confirm the previous analysis, but also provide more insights on the the specificity of the two opposite effects, PES and PEQ.

In Table 2 we compare the mean of the post-correct and post-error synaptic activities. The mean activity of the winning population is indistinguishable between post-correct and post-error trials. However, for short RSIs (corresponding to PES regime) the mean synaptic activities of the losing population are different for post-correct and post-error trials. Although the average activities of the winning population do not show statistically significant differences, the firing rates distributions are different, as shown on Extended Data Table 2-1 and Table 2-2).

RSI	Winning Population	Losing Population
500 ms	Fail to reject, $p = 0.16$	Reject, $p = 2.7 \times 10^{-20}$
2000 ms	Fail to reject, $p = 0.87$	Fail to reject, $p = 0.57$

Table 2: Table of the results for Unequal Variance (Welch) test, between the post-error / correct distributions of the synaptic activities at the time of the decision, with respect to the null hypothesis.

To get more insights, we plot in Fig. 15 the amplitude of the PES effect with respect to the inter-percentile range of the distribution of the synaptic activities of the winning and losing populations at the time of the previous decision. We note that when PES occurs, the higher the activity of the losing population at the time of decision, the stronger this effect will be. The influence of the winning population is observed, although in an opposite way. When PES occurs these effects are correlated (Dark Blue: Pearson correlation: $r = -0.98$ and $p = 2.6 \times 10^{-7}$, Medium Blue: $r = -0.98$ and $p = 9.5 \times 10^{-7}$), in the sense that the variations with respect to the inter-percentile of the winning and losing population are correlated. These observations are consistent with the analysis of the PES phase-plane trajectories. Indeed, the higher the losing population activity is, the closer to the invariant manifold the state at the end of the relaxation period will be. Hence, the effect will be stronger as it becomes easier (more likely) to cross the boundary.

However, we observe in Fig.15, panels A and C, a different behavior for the PEQ effect: there is an almost constant value of the PEQ effect with respect to the inter-percentiles of the distributions of the winning and losing populations activities. This is explained by the fact that, at the end of the relaxation, if the category of the new stimulus is the opposite of the previous decision, the network state finds itself within the (correct) associated basin of attraction, but very close from the boundary. This is true whatever the correctness of the previous decision. However, the post-correct case will lead to an even closer location from the basin boundary. The nonlinearity of the dynamics near the basin boundary will strongly amplify the small difference between post-correct and post-error ending point. The PEQ effect will thus not be correlated with the size of this difference.

For what concerns the PIA effect, we observe in Figure. 15.C-D a similar dependency in the synaptic activities as for the PES effect, with a stronger effect for high activities of the losing population. This corroborates the above phase plane analysis of the trajectories (Fig. 13). Indeed, the PES and PIA effects both depend on the position of the relaxation in the phase plane. Being closer to the boundary (high activity of the losing population) leads to a smaller error rate at the next trial.

Discussion

We have shown that an attractor neural network accounts, qualitatively and with the correct orders of magnitude, for sequential effects and post-error adjustments reported in experiments in the absence of any feedback about the correctness of the decision.

We provide evidence that these effects all result from the same intrinsic properties of the nonlinear neural decision dynamics, as detailed in the paper, and summarized below. We present in Figure 16 a schematic diagram of the occurrence of the effects depending on the parameters, even though this does not exhaust the richness of the systems behavior as discussed above.

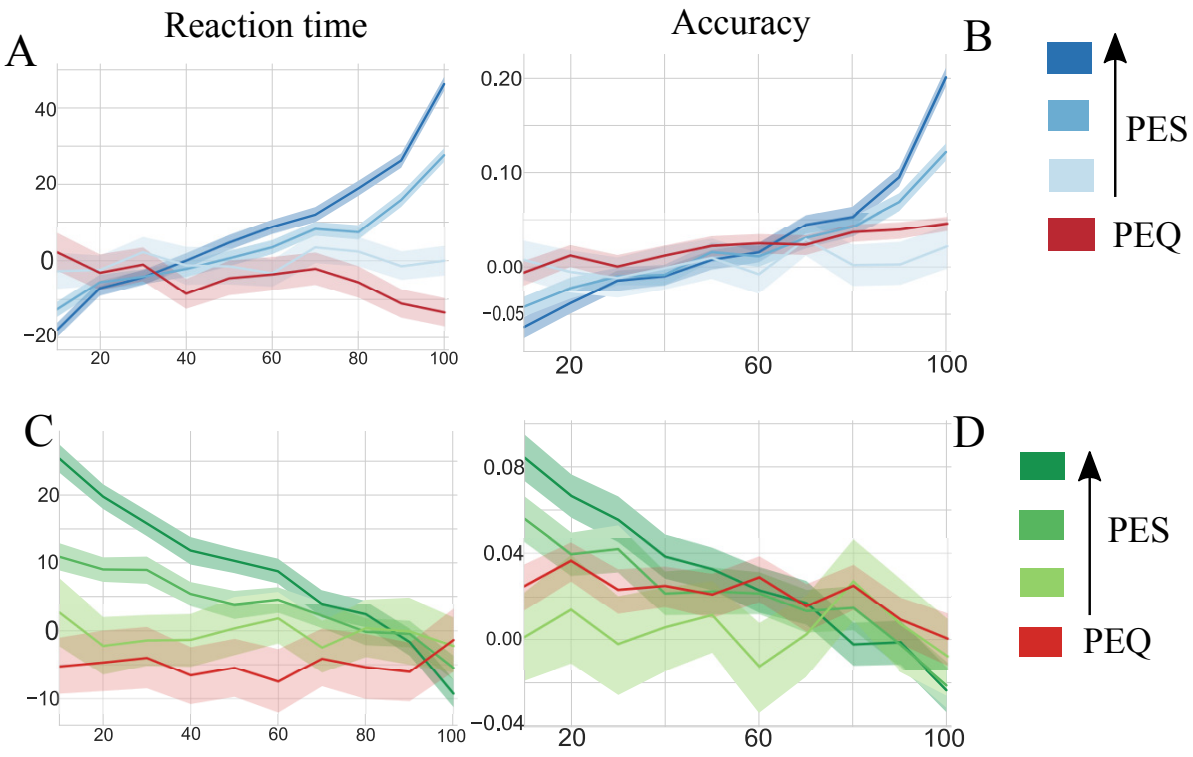

Figure 15: **Influence of the losing and winning population on the post-error adjustments.** *Panels (A) and (B) represents respectively the PES and PIA effect with respect to inter-percentiles range of the losing population synaptic activity distribution, at a RSI of* 500 *ms. The red curve corresponds to* $c = 18$ *and* $I_{CD,max} = 0.047$*, where we observe PEQ. Dark blue corresponds to strong PES effect (*$c = 10$*,* $I_{CD,max} = 0.035$*), medium blue to medium PES effect (*$c = 5$*,* $I_{CD,max} = 0.05$*). Light blue corresponds to no effect at all (*$c = 10$*,* $I_{CD,max} = 0.035$*), for a RSI of* 2 *seconds. Panels (C) and (D) represent the same curves for the winning population, with the same color code. The shadow area represents the* 95% *bootstrapped confidence intervals of the corresponding effect.*

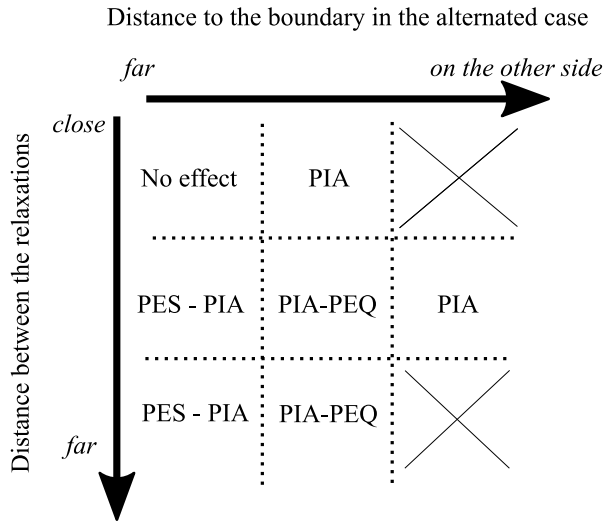

Figure 16: **Schematic diagram of the post-error adjustments observations.** *The x-axis represents the distance between the ending state of the relaxations and the boundary of the following basins of attraction. It goes from "the ending states are far away from the boundary" to "both ending states are in correct basin of attraction". The y-axis corresponds to the distance between the post-error and post-correct relaxations. The crosses denote regions which are not relevant, or inside which the network do not commit errors.*

Explanations for post-error slowing

Several cognitive explanations have been proposed to explain PES (Rabbitt and Rodgers, 1977; Laming, 1979a; Notebaert et al., 2009). They have been discussed in the framework of drift diffusion models (Dutilh et al., 2011; Goldfarb et al., 2012). Purcell and Kiani (2016) have studied PES and PEQ in human and monkeys in protocols with feedback about the correctness of the decision. They find that reaction times and accuracy can be fitted assuming DDM models with different parameters depending on the subject, and for a given subject calibrating separately on post-error and post-correct trials. Dutilh et al. (2011) show that, in behavioral experiments without feedback, modification of the response threshold within the DDM framework, would correspond to the hypothesis of increased response caution, the decision becoming less cautious after a correct response and more cautious after an error. In addition, they show that post-error and post-correct trials can be fitted by drift-diffusion models with different starting points. Yet, the neural correlates, which would determine the threshold or the starting point remain obscure, especially in the absence of explicit feedback on the correctness of the trial.

We are not aware of experimental studies of the neural correlates of PES and PEQ effects in the absence of feedback about the correctness of the decision. We note however that the neurophysiological data presented in Purcell and Kiani (2016) show, for experiments with feedback, neural activities at the beginning of a trial which are higher in case of PEQ, in agreement with our model.

Within the attractor neural network considered here, the PES and PEQ effects are explained thanks to a thorough analysis of the neural dynamics. Depending on the coherence level, the non-linearity of the system leads to different relative locations of the ending point of the relaxation (before the presentation of a new stimulus) with respect to the basins of attraction of the attractors induced by the next trial stimulus. Moreover, the difference in ending points, between post-error and post-correct cases, are amplified by the nonlinear dynamics during the next trial. An additional outcome of the analysis is that, for a given set of parameter values, different regimes (PES, PEQ or no effect) may be observed depending on the coherence level of the stimulus. Such properties cannot be obtained with linear models such as DDMs.

First and higher order sequential effects

Sequential effects can be categorized as first order (if caused by the immediately previous trial), or higher order (if caused by earlier trials in the sequence) (Laming, 1979b; Soetens et al., 1984, 1985; Cho et al., 2002). Post-error adjustments have also been experimentally observed at higher order (see Laming (1979b)).

Within the framework of attractor networks, the sequential effects in choice repetitions are explained by a starting bias, as discussed in Gao et al. (2009); Bonaiuto et al. (2016) and in the present paper. As stated by Gao et al. (2009), without any additional memory neural module, an attractor network has trouble in reproducing the transition between automatic facilitation and strategic expectancy (Laming, 1968). In our network, for too short RSIs (a few dozens of milliseconds) the sequential effects are too strong to be plausible. Decision conflict mechanisms (Jones et al., 2002) could be implement to correct this effect and to investigate other effects of repetitions and alternations (Gao et al., 2009).

To account for higher order effects, Gao et al. (2009) have introduced a dynamical network composed of four interacting modules. One is an attractor decision network module based on (Usher and McClelland, 2001) (a model more directly related to diffusion models than to biophysical models), and of memory units specific to alternated and repeated successive trials. This network is thus explicitly set up in such a way that it can reproduce automatic facilitation and strategic expectancy effects. In this model, even the first order effects result from a coupling between a short-term memory module and the decision network. In contrast, we have shown here that a decision attractor network model, without memory units, presents these first order effects as an intrinsic property of the dynamics.

However, due to the nature of the dynamics in our model, we do not expect to reproduce higher-order effects. Indeed, for parameters for which our model exhibits first order sequential effects (RSI of 1.5 second and $I_{CD,max} = 0.035$ nA), we find that the reaction time distributions for a sequence length of 2 or 1 are indistinguishable (repeated case, Smirnov-Kolmogorov test: $p = 0.28$, alternated case, Smirnov-Kolmogorov test: $p = 0.65$). Similarly we find no post-error adjustments, as illustrated in Figure 11-2 presenting the results of a systematic study in the space (c, $I_{CD,max}$).

One may ask whether a more complex architecture, taking into account other areas, could account for higher order repetition biases and post-error adjustments effects as resulting from some intrinsic properties of the dynamics, in the absence of specific memory units. Such architecture may then provide the basis of Bayesian inference as implemented in, e g, the LATER model Kim et al. (2017).

Working memory and Decision-Making

In this work we have considered *free response time task* (Roitman and Shadlen, 2002) in which the subject must make a decision as soon as possible. In the different protocol called *delayed visual motion discrimination experiment* (Shadlen and Newsome, 2001), the subject must make the decision at a prescribed time after the onset of the stimulus. In such task, the decision choice must be stored in order to be retrieved at the prescribed instant of time. In the original model of attractor neural network (Wang (2002); Wong and Wang (2006)), the decision is stored as in a working memory. As already discussed at the beginning of this paper, within the framework of a single module of attractor decision network, the implementation of the corollary discharge considered in the present paper allows the system to make successive decisions, at the price of removing the working memory behavior. An important issue is to understand how the decision making system can adapt itself to these opposite contexts. It is not unrealistic to expect a control mechanism onto the inhibitory current. Depending on the task, the inhibitory current could be sent either just after the decision has been made, or later after the end of the delay period. In the later case, a prediction is that, compared to cases without delay, there should be weaker post-error effects, but stronger repeated/alternated effects.

An alternative to such control mechanism is to have a more complex architecture. However, the memory units in Gao et al. (2009) are not appropriate for dealing with delayed discrimination experiments. For experiments with delays, Murray et al. (2017) consider two interacting modules, one implementing the posterior parietal cortex and an other one the posterior frontal cortex. Still, it is not clear if this system can deal with sequences of trials. It will be interesting to extend the present work by adding a working memory module in line with Murray et al. (2017), in order to obtain a network performing sequential decision-making while keeping the working memory behavior.

Finally we note that various brain areas have been shown to be involved in sequential decision tasks in which the memory of the last decision has to be maintained (Middlebrooks and Sommer, 2012; Donahue et al., 2013; Abzug and Sommer, 2018). This suggests more generally that a broader network is necessary for decision tasks requiring memory.

Future Prospects

During behavioral tasks, subjects are not always aware of their mistakes (Yeung and Summerfield, 2012), but do show post-error slowing. One may thus ask why one does not generally become aware that an error has been made, since the neural dynamics is different following an error or a success. As discussed in the present work, these differences in the dynamics are very subtle. The post-error and post-correct firing rates have broad distributions, with some common properties (the same mean for example). The strong overlapping of these distributions (see Fig. 15) makes it difficult to infer the correctness of the decision on a single trial basis. Yet, the tails of the post-error synaptic distribution should allow in some cases to infer that an error has been made. It would be interesting to see in behavioral experiments whether the post-error effects can be related to the confidence in one's decision (Wei et al., 2015; Insabato et al., 2017).

Our results also suggest to test experimentally the general picture resulting from our analysis, summarized in Fig. 16. In particular, some specific effects could be tested, such as post-error quickening at large coherence level, the properties of the discrimination threshold distribution in PIA, or the specific variations of post-error adjustments with respect to coherence levels.

Conflict of Interest

The authors declare no competing financial interests.

Acknowledgments

We thank Jerôme Sackur, Jean-Rémy Martin and Laurent Bonnasse-Gahot for useful discussions. KB acknowledges a fellowship from the ENS Paris-Saclay.

References

Abbott, L. F. and Chance, F. S. (2005). Drivers and modulators from push-pull and balanced synaptic input. In *Progress in Brain Research*, volume 149, pages 147–155.

Abzug, Z. M. and Sommer, M. A. (2018). Serial decision-making in monkeys during an oculomotor task. *Journal of Experimental Psychology: Animal Learning and Cognition*, 44(1):95–102.

Ashby, F. (1983). A biased random walk model for two choice reaction times. *Journal of Mathematical Psychology*, 27(3):277–297.

Benjamin, D. J., Berger, J. O., Johannesson, M., Nosek, B. A., Wagenmakers, E.-J., Berk, R., Bollen, K. A., Brembs, B., Brown, L., Camerer, C., Cesarini, D., Chambers, C. D., Clyde, M., Cook, T. D., De Boeck, P., Dienes, Z., Dreber, A., Easwaran, K., Efferson, C., Fehr, E., Fidler, F., Field, A. P., Forster, M., George, E. I., Gonzalez, R., Goodman, S., Green, E., Green, D. P., Greenwald, A. G., Hadfield, J. D., Hedges, L. V., Held, L., Hua Ho, T., Hoijtink, H., Hruschka, D. J., Imai, K., Imbens, G., Ioannidis, J. P. A., Jeon, M., Jones, J. H., Kirchler, M., Laibson, D., List, J., Little, R., Lupia, A., Machery, E., Maxwell, S. E., McCarthy, M., Moore, D. A., Morgan, S. L., Munafó, M., Nakagawa, S., Nyhan, B., Parker, T. H., Pericchi, L., Perugini, M., Rouder, J., Rousseau, J., Savalei, V., Schönbrodt, F. D., Sellke, T., Sinclair, B., Tingley, D., Van Zandt, T., Vazire, S., Watts, D. J., Winship, C., Wolpert, R. L., Xie, Y., Young, C., Zinman, J., and Johnson, V. E. (2018). Redefine statistical significance. *Nature Human Behaviour*, 2:6–10.

Bezanson, J., Edelman, A., Karpinski, S., and Shah, V. B. (2014). Julia: A Fresh Approach to Numerical Computing. *SIAM REVIEW*, 59(1):65–98.

Bliss, D. P. and D'Esposito, M. (2017). Synaptic augmentation in a cortical circuit model reproduces serial dependence in visual working memory. *PLoS ONE*, 12(12):7–10.

Bogacz, R. (2009). Optimal decision making theories. In *Handbook of reward and decision making*, pages 375–397. Academic Press.

Bonaiuto, J. J., De Berker, A., and Bestmann, S. (2016). Response repetition biases in human perceptual decisions are explained by activity decay in competitive attractor models. *eLife*, 5.

Busemayer, J. R. and Townsend, J. T. (1993). Decision field theory: A dynamics-cognitive approach to desion making in an uncertain environment. *Psychological Review*, 100(3):432–459.

Cho, R. Y., Nystrom, L. E., Brown, E. T., Jones, A. D., Braver, T. S., Holmes, P. J., and Cohen, J. D. (2002). Mechanisms underlying dependencies of performance on stimulus history in a two-alternative forced-choice task. *Cognitive, Affective and Behavioral Neuroscience*, 2(4):283–299.

Cohen, M. X. (2009). Unconscious errors enhance prefrontal-occipital oscillatory synchrony. *Frontiers in Human Neuroscience*, 3(November):1–12.

Compte, a., Brunel, N., Goldman-Rakic, P. S., and Wang, X. J. (2000). Synaptic mechanisms and network dynamics underlying spatial working memory in a cortical network model. *Cerebral cortex (New York, N.Y. : 1991)*, 10(9):910–23.

Crapse, T. B. and Sommer, M. A. (2008). Corollary discharges across the animal kingdom. *Nat Rev Neurosci*, 9(AuguST):587–600.

Crapse, T. B. and Sommer, M. A. (2009). Frontal Eye Field Neurons with Spatial Representations Predicted by Their Subcortical Input. *Journal of Neuroscience*, 29(16):5308–5318.

Danielmeier, C. and Ullsperger, M. (2011). Post-error adjustments. *Frontiers in Psychology*, 2(SEP):1–10.

Debener, S. (2005). Trial-by-Trial Coupling of Concurrent Electroencephalogram and Functional Magnetic Resonance Imaging Identifies the Dynamics of Performance Monitoring. *Journal of Neuroscience*, 25(50):11730–11737.

Deco, G., Ponce-Alvarez, A., Mantini, D., Romani, G. L., Hagmann, P., and Corbetta, M. (2013). Resting-State Functional Connectivity Emerges from Structurally and Dynamically Shaped Slow Linear Fluctuations. *Journal of Neuroscience*, 33(27):11239–11252.

Ding, L. and Hikosaka, O. (2006). Comparison of Reward Modulation in the Frontal Eye Field and Caudate of the Macaque. *Journal of Neuroscience*, 26(25):6695–6703.

Donahue, C. H., Seo, H., and Lee, D. (2013). Cortical Signals for Rewarded Actions and Strategic Exploration. *Neuron*, 80(1):223–234.

Dutilh, G., Vandekerckhove, J., Forstmann, B. U., Keuleers, E., Brysbaert, M., and Wagenmakers, E.-J. (2011). Testing theories of post-error slowing. *Attention, Perception, & Psychophysics*, 74(2):454–465.

Efron, B. and Tibshirani, R. J. (1994). *An Introduction to the Bootstrap*. CRC Press.

Engel, T. A., Chaisangmongkon, W., Freedman, D. J., and Wang, X. J. (2015). Choice-correlated activity fluctuations underlie learning of neuronal category representation. *Nature Communications*, 6.

Engel, T. A. and Wang, X.-J. (2011). Same or Different? A Neural Circuit Mechanism of Similarity-Based Pattern Match Decision Making. *Journal of Neuroscience*, 31(19):6982–6996.

Ermentrout, G. B. and Mahajan, A. (2003). *Simulating, Analyzing, and Animating Dynamical Systems: A Guide to XPPAUT for Researchers and Students*, volume 56.

Farrell, S. and Ludwig, C. J. H. (2008). Bayesian and maximum likelihood estimation of hierarchical response time models. *Psychonomic Bulletin & Review*, 15(6):1209–1217.

Fecteau, J. H. and Munoz, D. P. (2003). Exploring the consequences of the previous trial. *Nature Reviews Neuroscience*, 4(6):435–443.

Finkel, A. S. and Redman, S. J. (1983). The synaptic current evoked in cat spinal motoneurones by impulses in single group 1a axons. *The Journal of Physiology*, 342(1):615–632.

Fleming, S. M. (2010). Relatiing Introspective Accuracy to Individual Differences in Brain Structure. *Science*, 1541(September 2010):1541–1544.

Ganguli, S., Bisley, J. W., Roitman, J. D., Shadlen, M. N., Goldberg, M. E., and Miller, K. D. (2008). One-Dimensional Dynamics of Attention and Decision Making in LIP. *Neuron*, 58(1):15–25.

Gao, J., Wong-Lin, K., Holmes, P., Simen, P., and Cohen, J. D. (2009). Sequential effects in two-choice reaction time tasks: decomposition and synthesis of mechanisms. *Neural computation*, 21(9):2407–36.

Gehring, W. J. and Fencsik, D. E. (2001). Functions of the medial frontal cortex in the processing of conflict and errors. *The Journal of Neuroscience*, 21(23):9430–9437.

Goldfarb, S., Wong-Lin, K. F., Schwemmer, M., Leonard, N. E., and Holmes, P. (2012). Can post-error dynamics explain sequential reaction time patterns? *Frontiers in Psychology*, 3(JUL).

Hall, W. C. and Moschovakis, A. K. (2003). *The superior colliculus: new approaches for studying sensorimotor integration*. CRC Press.

Hester, R., Foxe, J. J., Molholm, S., Shpaner, M., and Garavan, H. (2005). Neural mechanisms involved in error processing: A comparison of errors made with and without awareness. *NeuroImage*, 27(3):602–608.

Hollander, M., Wolfe, D. A., and Chicken, E. (2014). *Nonparametric statistical methods.*, volume 2. Wiley Series in Probability and Statistics.

Insabato, A., Pannunzi, M., and Deco, G. (2017). Multiple Choice Neurodynamical Model of the Uncertain Option Task. *PLoS Computational Biology*, 13(1).

Jentzsch, I. and Dudschig, C. (2009). Why do we slow down after an error? Mechanisms underlying the effects of posterror slowing. *Quarterly Journal of Experimental Psychology*, 62(2):209–218.

Jones, A. D., Cho, R. Y., Nystrom, L. E., Cohen, J. D., and Braver, T. S. (2002). A computational model of anterior cingulate function in speeded response tasks: Effects of frequency, sequence, and conflict. *Cognitive, Affective and Behavioral Neuroscience*, 2(4):300–317.

Kim, T. D., Kabir, M., and Gold, J. I. (2017). Coupled Decision Processes Update and Maintain Saccadic Priors in a Dynamic Environment. *The Journal of Neuroscience*, 37(13):3632–3645.

King, J. A., Korb, F. M., von Cramon, D. Y., and Ullsperger, M. (2010). Post-Error Behavioral Adjustments Are Facilitated by Activation and Suppression of Task-Relevant and Task-Irrelevant Information Processing. *Journal of Neuroscience*, 30(38):12759–12769.

Laming, D. (1979a). Autocorrelation of choice-reaction times. *Acta Psychologica*, 43(5):381–412.

Laming, D. (1979b). Choice reaction performance following an error. *Acta Psychologica*, 43(3):199–224.

Laming, D. R. J. (1968). Information theory of choice-reaction times. *Information theory of choicereaction times*, 14:172.

Lauwereyns, J., Watanabe, K., Coe, B., and Hikosaka, O. (2002). A neural correlate of response bias in monkey caudate nucleus. *Nature*, 418(JULY):413–417.

Lo, C. C. and Wang, X. J. (2006). Cortico-basal ganglia circuit mechanism for a decision threshold in reaction time tasks. *Nature Neuroscience*, 9(7):956–963.

Marco-Pallarés, J., Camara, E., Münte, T. F., and Rodríguez-Fornells, A. (2008). Neural mechanisms underlying adaptive actions after slips. *Journal of Cognitive Neuroscience*, 20(9):1595–610.

Middlebrooks, P. G. and Sommer, M. A. (2012). Neuronal correlates of metacognition in primate frontal cortex Paul. *Neuron*, 75(3):517–530.

Miller, P. and Katz, D. B. (2013). Accuracy and response-time distributions for decision-making: linear perfect integrators versus nonlinear attractor-based neural circuits. *Journal of Computational Neuroscience*, 35:261–294.

Murray, J. D., Jaramillo, J., and Wang, X.-J. (2017). Working memory and decision making in a fronto-parietal circuit model. *Journal of Neuroscience*, 37(50):12167–12186.

Notebaert, W., Houtman, F., Opstal, F. V., Gevers, W., Fias, W., and Verguts, T. (2009). Post-error slowing: An orienting account. *Cognition*, 111(2):275–279.

Núñez Castellar, E., Kühn, S., Fias, W., and Notebaert, W. (2010). Outcome expectancy and not accuracy determines posterror slowing: ERP support. *Cognitive, Affective and Behavioral Neuroscience*, 10(2):270–278.

Padoa-Schioppa, C. (2013). Neuronal origins of choice variability in economic decisions. *Neuron*, 80(5):1322–1336.

Purcell, B. A. and Kiani, R. (2016). Neural Mechanisms of Post-error Adjustments of Decision Policy in Parietal Cortex. *Neuron*, 89(3):658–671.

Quick, R. F. (1974). A vector-magnitude model of contrast detection. *Kybernetik*, 16(2):65–67.

Rabbitt, P. and Rodgers, B. (1977). What does a man do after he makes an error? an analysis of response programming. *Quarterly Journal of Experimental Psychology*, 29(4):727–743.

Rao, V., DeAngelis, G. C., and Snyder, L. H. (2012). Neural Correlates of Prior Expectations of Motion in the Lateral Intraparietal and Middle Temporal Areas. *Journal of Neuroscience*, 32(29):10063–10074.

Ratcliff, R. (1978). A theory of memory retrieval. *Psychological Review*, 85(2):59–108.

Ratcliff, R. (2004). A Comparison of Sequential Sampling Models for Two-Choice Reaction Time Roger Ratcliff Northwestern University Philip L . Smith University of Melbourne. *Psychological Review*, 111(2):333–367.

Ratcliff, R. and McKoon, G. (2008). The Diffusion Decision Model: Theory and Data for Two-Choice Decision Tasks. *Neural Computation*, 20(4):873–922.

Rizzo, M. and Székely, G. (2014). Energy: E-statistics (energy statistics). R package version 1.6.2.

Rizzo, M. L. and Székely, G. J. (2016). Energy distance. *Wiley Interdisciplinary Reviews: Computational Statistics*, 8(1):27–38.

Roitman, J. D. and Shadlen, M. N. (2002). Response of neurons in the lateral intraparietal area during a combined visual discrimination reaction time task. *Journal of Neuroscience*, 22(21):9475–9489.

Saito, Y. and Isa, T. (2003). Local excitatory network and NMDA receptor activation generate a synchronous and bursting command from the superior colliculus. *The Journal of neuroscience : the official journal of the Society for Neuroscience*, 23(13):5854–5864.

Scudder, C. A., Kaneko, C. R., and Fuchs, A. F. (2002). The brainstem burst generator for saccadic eye movements: A modern synthesis. *Experimental Brain Research*, 142(4):439–462.

Shadlen, M. N., Hanks, T. D., Churchland, A. K., Kiani, R., and Yang, T. (2006). The Speed and Accuracy of a Simple Perceptual Decision: A Mathematical Primer. *Bayesian Brain: Probabilistic Approaches to Neural Coding*, pages 207–233.

Shadlen, M. N. and Newsome, W. T. (1996). Motion perception: seeing and deciding. *Proceedings of the National Academy of Sciences of the United States of America*, 93(January):628–633.

Shadlen, N. N. and Newsome, W. T. (2001). Neural basis of a perceptual decision in the parietal cortex (area lip) of the rhesus monkey. *Journal of Neurophysiology*, 86:1916–1936.

Shorack, G. R. and Wellner, J. A. (2009). *Empirical processes with applications to statistics*. Siam.

Soetens, E., Boer, L. C., and Hueting, J. E. (1985). Expectancy or Automatic Facilitation? Separating Sequential Effects in Two-Choice Reaction Time. *Journal of Experimental Psychology: Human Perception and Performance*, 11(5):598–616.

Soetens, E., Deboeck, M., and Hueting, J. (1984). Automatic aftereffects in two-choice reaction time: A mathematical representation of some concepts. *Journal of Experimental Psychology: Human Perception and Performance*, 10(4):581–598.

Sommer, M. A. and Wurtz, R. H. (2008). Visual perception and corollary discharge. *Perception*, 37(3):408–418.

Szekely, G. and Rizzo, M. (2013). Energy statistics: statistics based on distances. *Journal of Statistical Planning and Inference*, 143(8):1249–1272.

Townsend, J. T. and Ashby, F. G. (1983). *The stochastic modeling of elementary psychological processes*. Cambridge University Press.

Usher, M. and McClelland, J. L. (2001). The time course of perceptual choice: The leaky, competing accumulator model. *Psychological Review*, 108(3):550–592.

Verguts, T., Notebaert, W., Kunde, W., and Wühr, P. (2011). Post-conflict slowing: Cognitive adaptation after conflict processing. *Psychonomic Bulletin and Review*, 18(1):76–82.

Vickers, D. (1979). *Decision processes in Visual Perception*. Academic Press.

Wang, X.-J. J. (2002). Probabilistic decision making by slow reverberation in cortical circuits. *Neuron*, 36(5):955–968.

Wei, W., Rubin, J. E., and Wang, X.-J. (2015). Role of the Indirect Pathway of the Basal Ganglia in Perceptual Decision Making. *Journal of Neuroscience*, 35(9):4052–4064.

Wong, K.-F., Huk, A. C., Shadlen, M. N., and Wang, X.-J. (2007). Neural circuit dynamics underlying accumulation of time-varying evidence during perceptual decision making. *Frontiers in Computational Neuroscience*, 1.

Wong, K.-F. and Wang, X.-J. (2006). A Recurrent Network Mechanism of Time Integration in Perceptual Decisions. *Journal of Neuroscience*, 26(4):1314–1328.

Yang, Y., Cao, P., Yang, Y., and Wang, S. R. (2008). Corollary discharge circuits for saccadic modulation of the pigeon visual system. *Nature Neuroscience*, 11(5):595–602.

Yeung, N. and Summerfield, C. (2012). Metacognition in human decision-making: confidence and error monitoring. *Philosophical Transactions of the Royal Society B: Biological Sciences*, 367(1594):1310–1321.

Extended Data

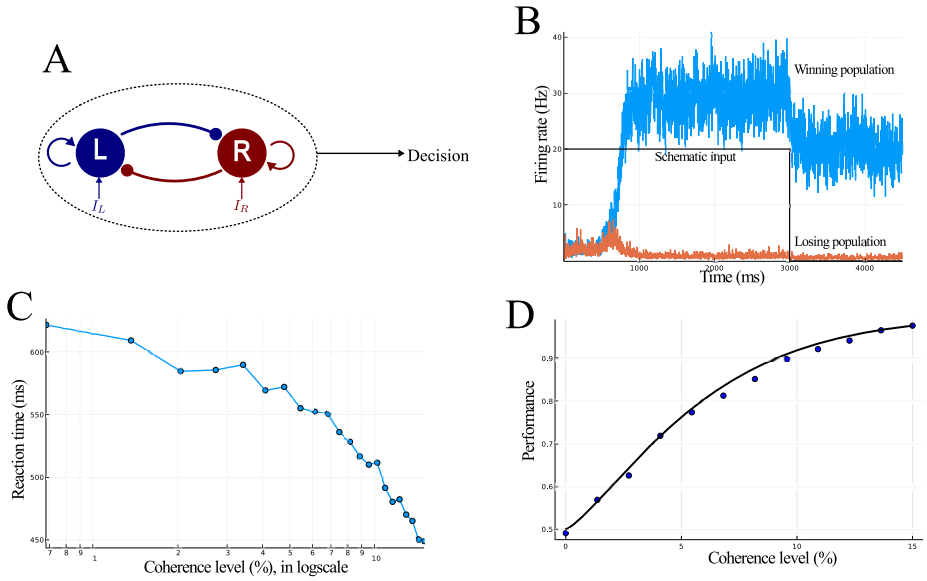

: **Figure 1-1: Wong and Wang two-variable model.** *(A) Reduced two-variable model constituted of two neural units, endowed with self-excitation and effective mutual inhibition. (B) Time course of the two neural activities during a decision-making task. At the beginning the two firing rates are indistinguishable. The firing rate that ramps upward (blue) represents the winning population, the orange one the losing population. A decision is made when one of the firing rate crosses the threshold of* 20 *Hz. The black line represents the duration of the selective input corresponding to the duration of accumulation of evidence until the decision threshold is reached. This model shows working memory through the persistent activity in the network after the decision is made. Panels (C) and (D), Model simulations on one virtual subject: (C) Mean reaction time in the decision task, and, (D) Performance, both in function of stimulus coherence (stimulus ambiguity).*

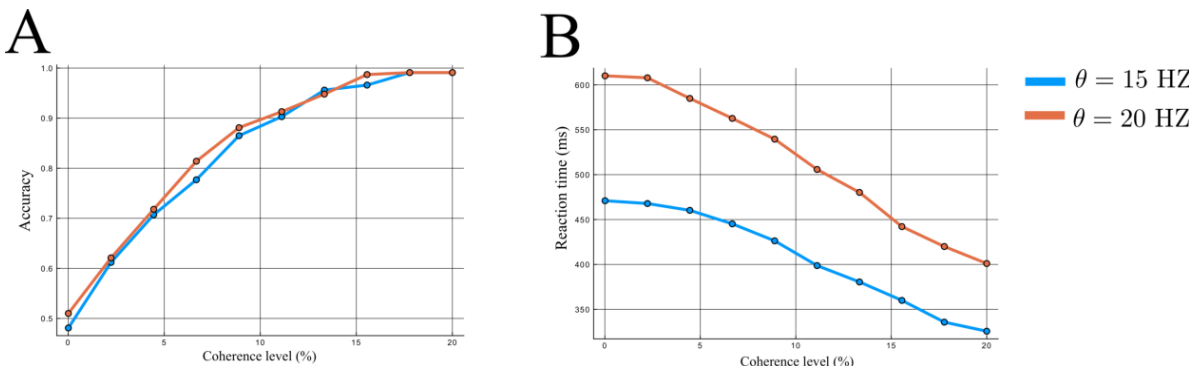

: **Figure 1-2: Psychometric and chronometric functions of the original network.** *(A): Accuracy of the model with respect to coherence levels. In blue we plot the $\theta = 15$ Hz case, and in orange the $\theta = 20$ Hz one. Data are obtained by averaging on 1000 trials. (B) Reaction time of the network, with the same color code. The network still performs decision-making in an analog way to the original model (as the motor reaction time is not taken into account and could be rescaled in a full model).*

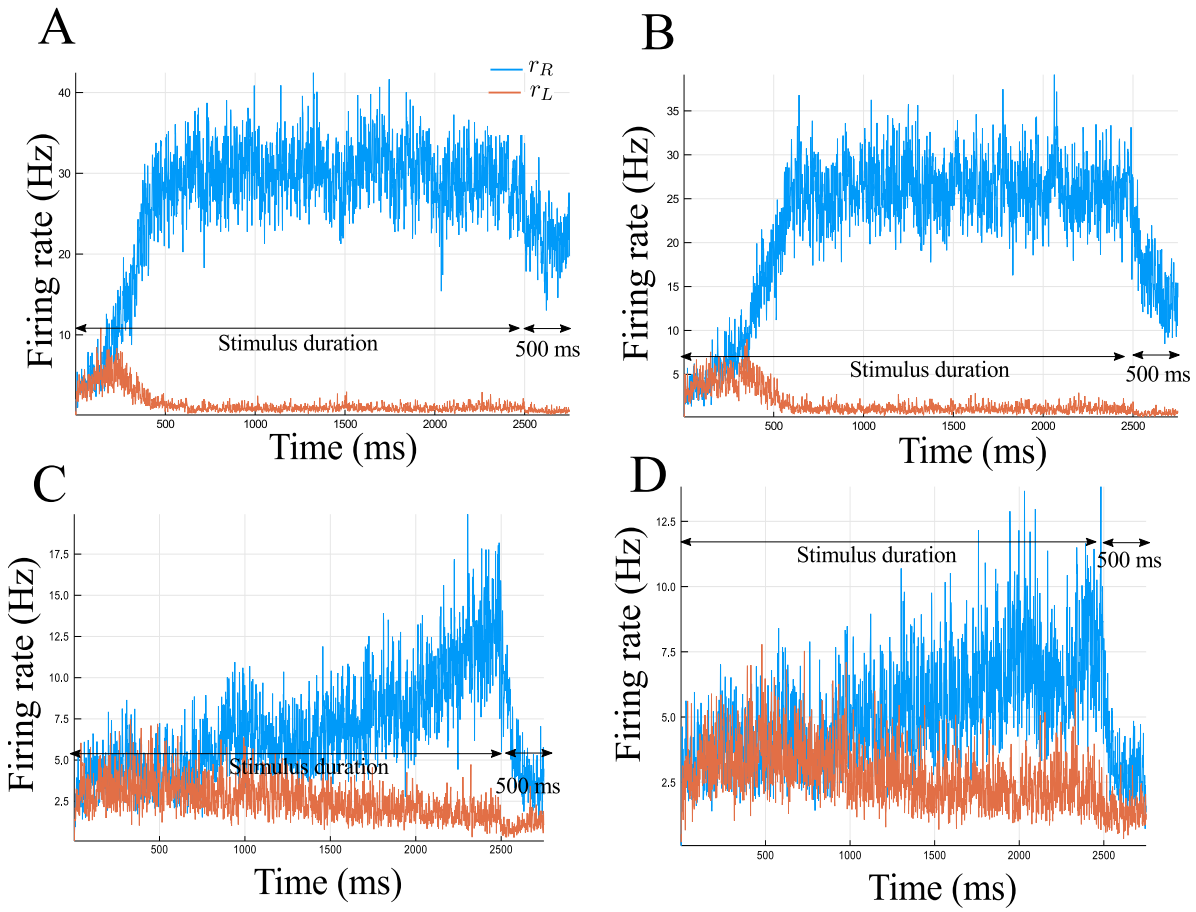

: **Figure 1-3: Simulations of the reduced attractor network without the CD input: dynamics with weaker recurrent excitatory weights.** *We perform simulations of the model with a fixed stimulus duration, and we observe the relaxation during a* 500 *ms period. Panel (A) corresponds to the original model, which do not hsow relaxation but working memory. Panel (B) corresponds to a slow relaxation (with* $J_{11} = J_{22} = 0.25$*), where after* 500 *ms the system is far from the neutral state. (C) The recurrent excitation is* $J_{11} = J_{22} = 0.22$*. The state of the system is still highly biased in the favor of the previous choice, and, most importantly, the reaction times are not coherent with behavioral data (more than* 2 *seconds). (D) The recurrent excitation is* $J_{11} = J_{22} = 0.215$*. We obtain a relaxation on a time-scale of* 500 *ms, but the network is not able to perform decision-making anymore as it does not cross the threshold.*

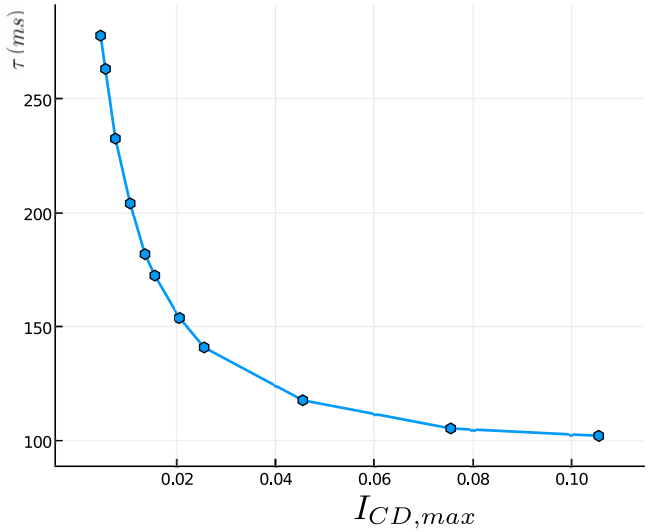

: **Table 1-1: Relaxation time constant.** *Relaxation time constant of the system during the RSI (that is the relaxation dynamics towards the neutral attractor state), with respect to the corollary discharge amplitude. The values are obtained by computing the eigenvalues of the dynamical system and using the relation* $\lambda = \frac{1}{\tau}$*, with* τ *the time constant.*

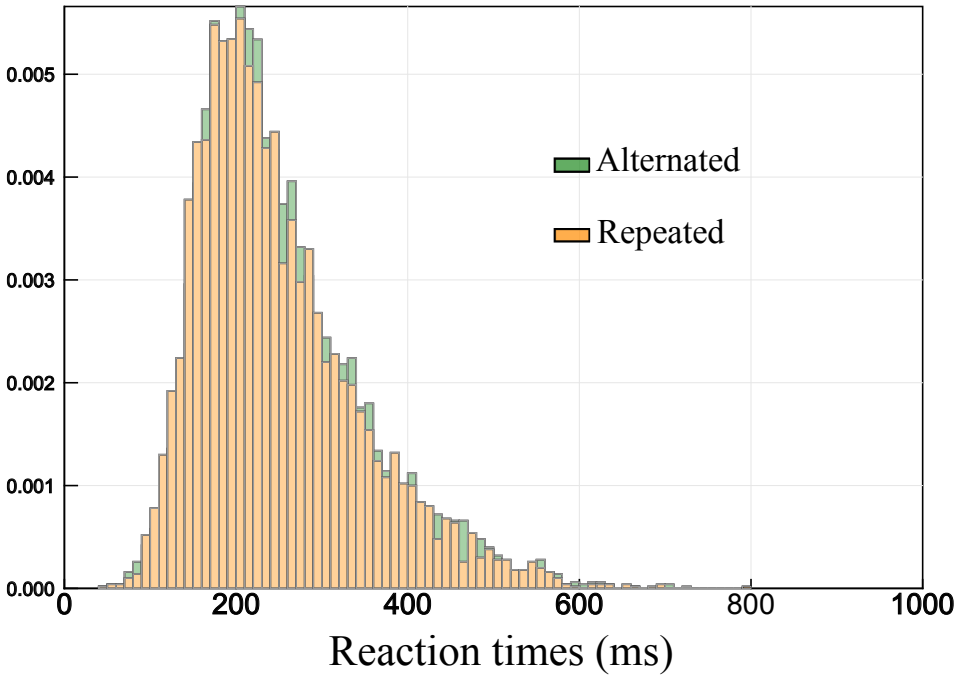

: **Figure 5-1: RSI of** 5 **seconds.** *Histogram of the reaction time for simulations with* $I_{CD,max} = 0.035$ *nA. The distributions of the reaction times of the two groups are indistinguishable (E-statistic test,* $p = 0.61$*). The distributions of the coherence levels in these two groups are indistinguishable (Anderson-Daring test:* $p = 0.53$*).*

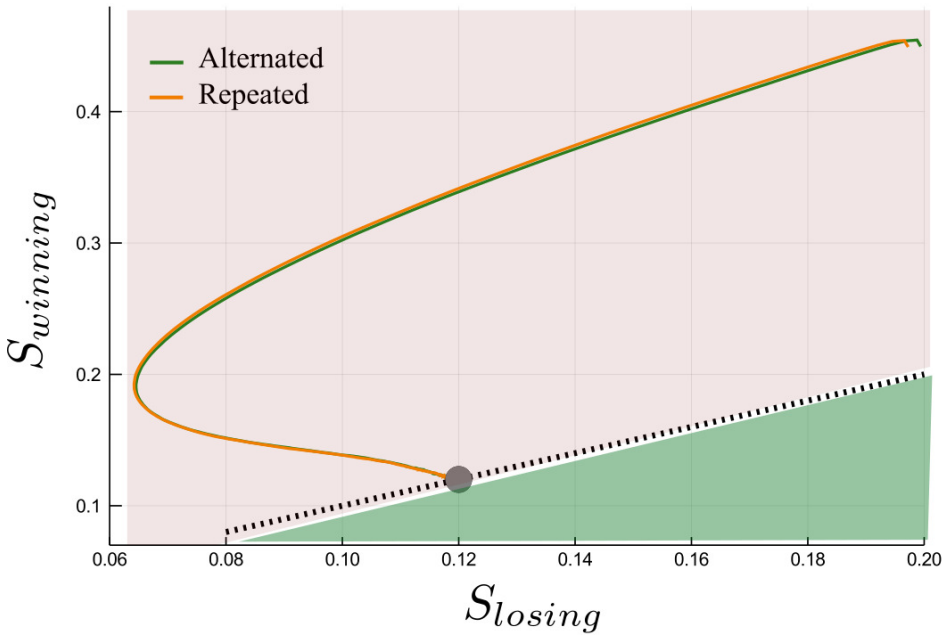

: **Figure 7-1: RSI of** 5 **seconds.** *Average dynamics between two successive trials in the phase-plane coordinates, during the* 500*ms preceding the onset of the next stimulus. Anderson-Darling test on the* 500 *ms prior to stimulus for the synaptic activities: for losing population* $p = 0.06$*, and for the winning population* $p = 0.03$*.*

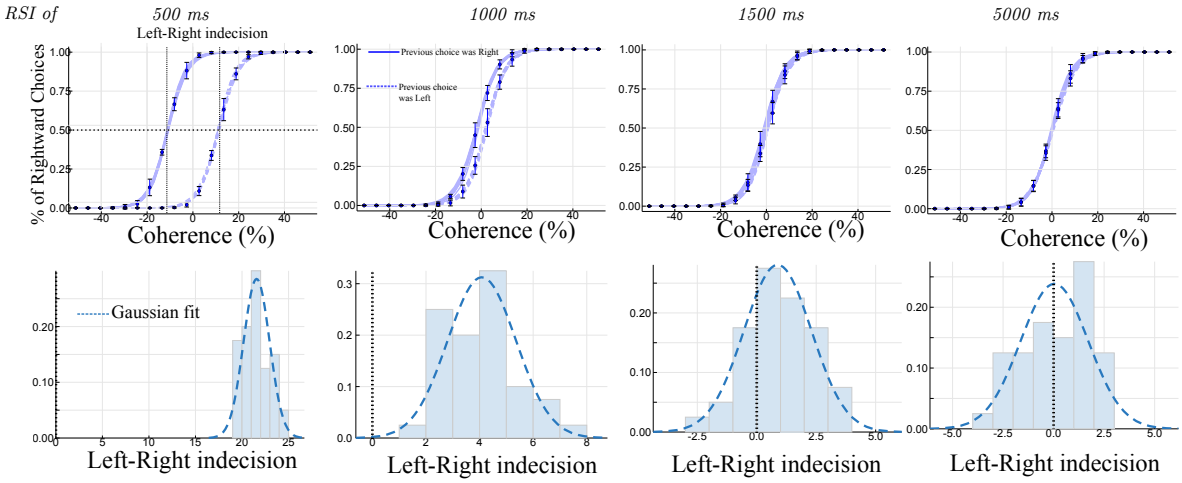

: **Figure 7-2: Repetition biases for several RSI values.** *Upper panel: percentage of Right choices, with respect to coherence level, depending on the previous choice (Left or Right). The blue points represents the mean accuracy (on 24 simulations) and the confidence interval at* 95% *(bootstrap method). The blue lines denote the fit (of all simulations) by a logistic regression of all (plain: previous choice was Right, dashed: previous choice was Left). Bottom panel: histogram of the Left-Right indecision point (on 24 simulations to stay in the experimental range). It characterizes the fact that the positive shift in the indecision point is increased for small RSI. The mean of the indecision point shift decreases with longer response-stimulus intervals.*

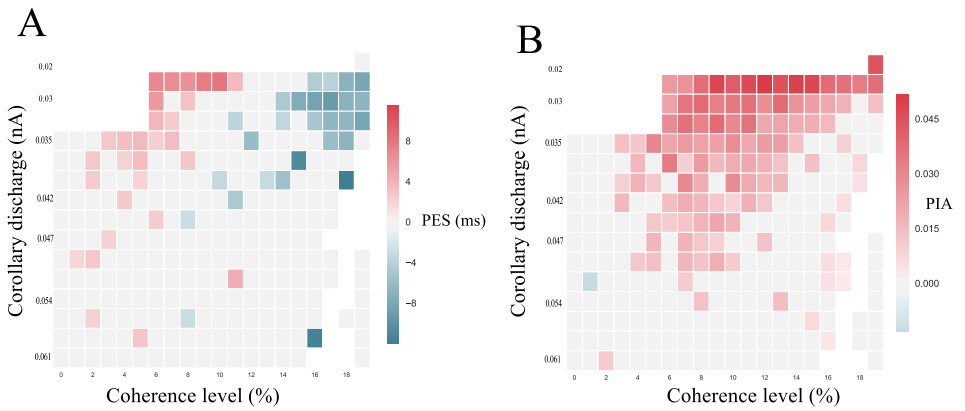

: **Figure 10-1: Post-error adjustments at $\tau_{CD} = 500$ ms.** *(A) Phase diagram of the PES effect at RSI of* 500 *ms. The bottom white zone corresponds to parameters where sequential decision-making is impossible. The red square corresponds to regions where PES is observed, and the blue ones where PEQ is observed. We used a bootstrapped confidence interval in order to decide whether or not PES (or PEQ) is observed. (B) Phase diagram of the PIA effect at RSI of* 500 *ms. The red square corresponds to regions where PIA is observed. We used a bootstrapped confidence interval in order to decide whether or not PIA is observed. The observation of post-error adjustments is highly impacted with the value of* τ_{CD}*, as we do not observe PES for the same range of parameters.*

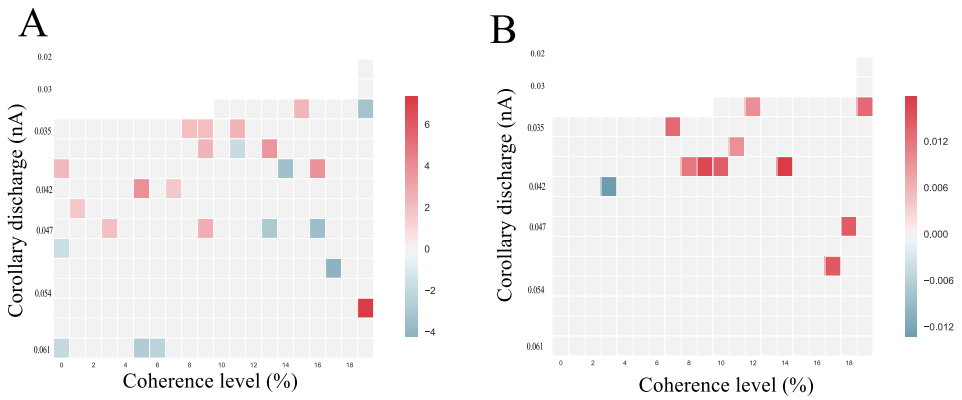

: **Figure 10-2: 2nd Order post-error adjustments**. *(A) Phase diagram of the PES effect at the* $n+2$ *trial. (B) Phase diagram of the PIA effect at the* $n+2$ *trial. For both panels: Simulations with a RSI of* 500 *ms, other parameters as in Table 1. The upper white zone corresponds to parameters where sequential decision-making is not possible. Color code as Figure 7 (main paper). One sees rare isolated red squares, indicating the absence of any systematic effect.*

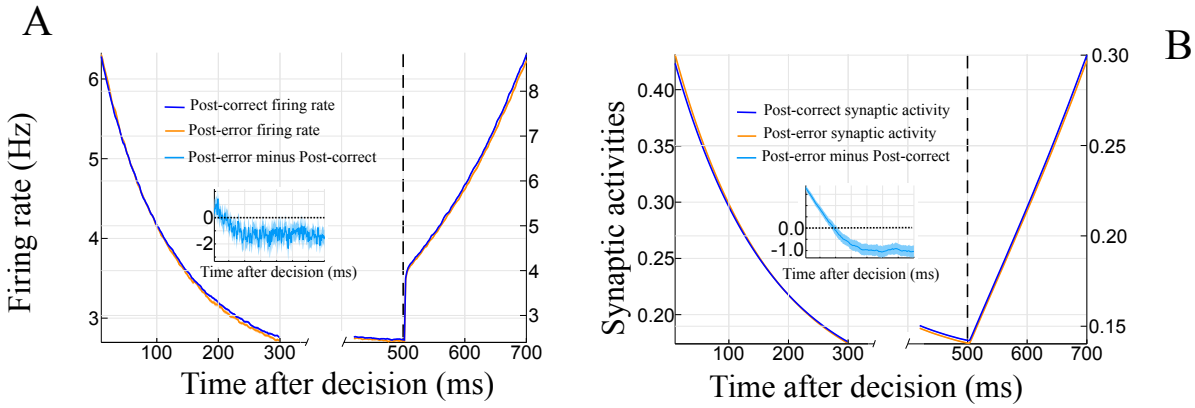

: **Figure 13-1: Mean firing rates of the winning population.** *(A) Mean firing rates for the winning populations of the next trial: in blue the post-correct case and in orange the post-error one. The ribbons represent the* 95% *confidence interval on 25 simulations(bootstrap method). The left-axis represents the relaxation of the dynamics. The right-axis is for the beginning of the new stimulus. The parameters are set to a region with PES effects (*$I_{CD} = 0.035$ *nA and* $c = \pm 10$*). The sub-panel with the light blue curve is the difference between the post-error firing rates and the post-correct with respect to time (in percent). The ribbon stands for the* 95% *confidence interval. As expected, this difference is negative. Hence the post-correct dynamics is faster and crosses sooner the threshold. This leads to the PES effect. (B) Mean synaptic activities for the winning populations of the next trial: in blue the post-correct case and in orange the post-error one. The ribbons represent the* 95% *confidence interval on 25 simulations(bootstrap method). The notations are the same as for the left figure.. The sub-panel with the light blue curve is the difference between the post-error synaptic activities and the post-correct with respect to time (in percent). The ribbon stands for the* 95% *confidence interval. This difference is less noisy than for the firing rates. However it possess the same behavior. When working with mean behavior of the network, we will now use the synaptic activities which are the main dynamical variables, and less noisy than the firing rates. Due to the similarity between the two variables the conclusions will not be affected.*

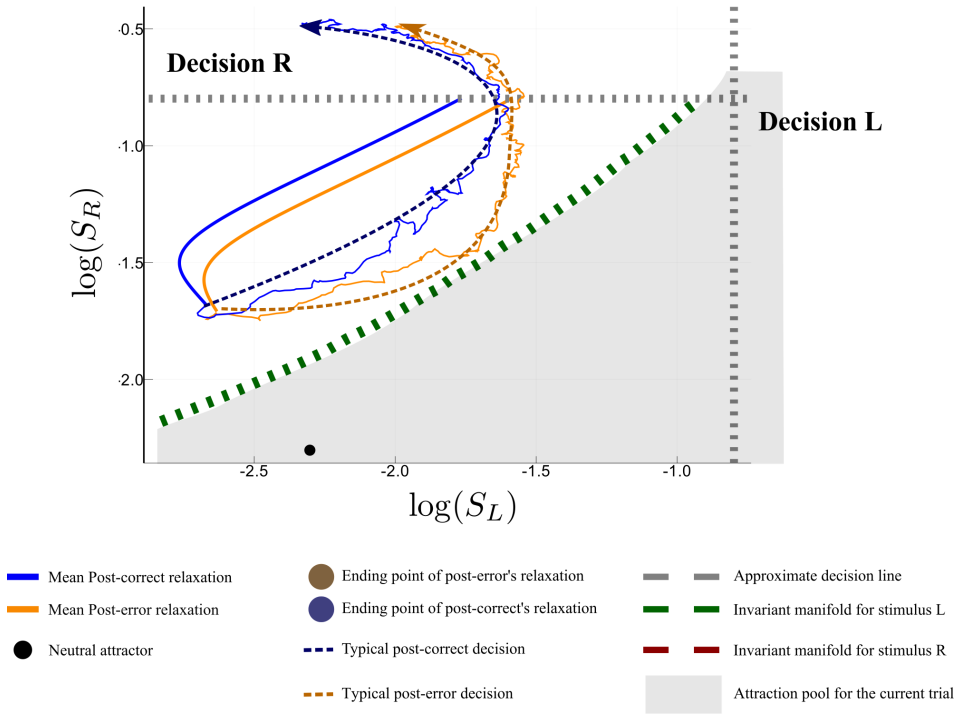

: **Figure 13-2: Analysis of the post-error trajectories for error trials.** *Phase-plane trajectories (in log-log plot, for ease of viewing) of the post-correct and post-error trials, for several regimes. We consider that the previous decision was decision R. The black circle shows the neutral attractor state (during the relaxation period). During the presentation of the next stimulus, the attractors and basins of attraction change. (represented by the gray area and the green or red dashed line). PES and PIA regime ($c = 10$ and $I_{CD,max} = 0.035$ nA). The blue color codes for post-correct trials, and the orange one for post-error. The arrows denote typical time dynamics for error trials when the choice must be L.*

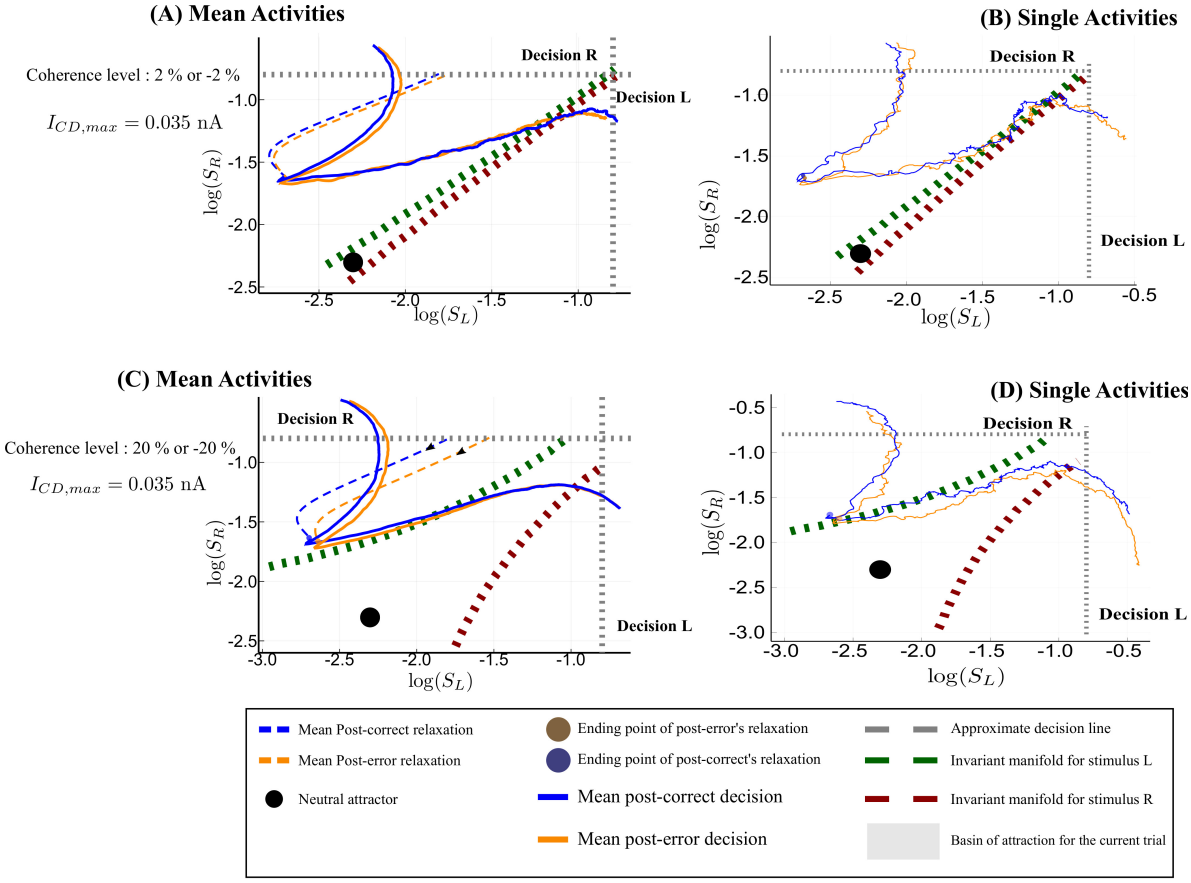

: **Figure 14-1: Analysis of the post-error trajectories in the regime with neither PES nor PEQ effect** *Phase-plane trajectories (in log-log plot, for ease of viewing) of the post-correct and post-error trials. We consider that the previous decision was decision R. The black filled circle shows the neutral attractor state (during the relaxation period). During the presentation of the next stimulus, the attractors and basins of attraction change (represented by the gray area and the green or red dashed line). Panels (A) (mean dynamics) and (B) (single dynamics): regime without PES or PIA ($c = \pm 2\%$ and $I_{CD,max} = 0.035$ nA). We show both the alternated and the repeated case, with the corresponding basins of attraction. The blue color codes for post-correct trials, and the orange one for post-error. For alternated trials, the dynamics needs to cross the invariant manifold (green dashed line), which denotes the boundary between the basins of attraction. Panels (C) (mean dynamics) and (D) (single dynamics): regime with PIA but without PES ($c = \pm 20\%$ and $I_{CD,max} = 0.035$ nA). The dynamics is followed during 400ms for repeated and 800 ms for alternated case, as if there were no decision threshold. The actual decision occurs at the crossing of the dashed gray line, indicating the threshold. This allows to visually compare the associated reaction times.*

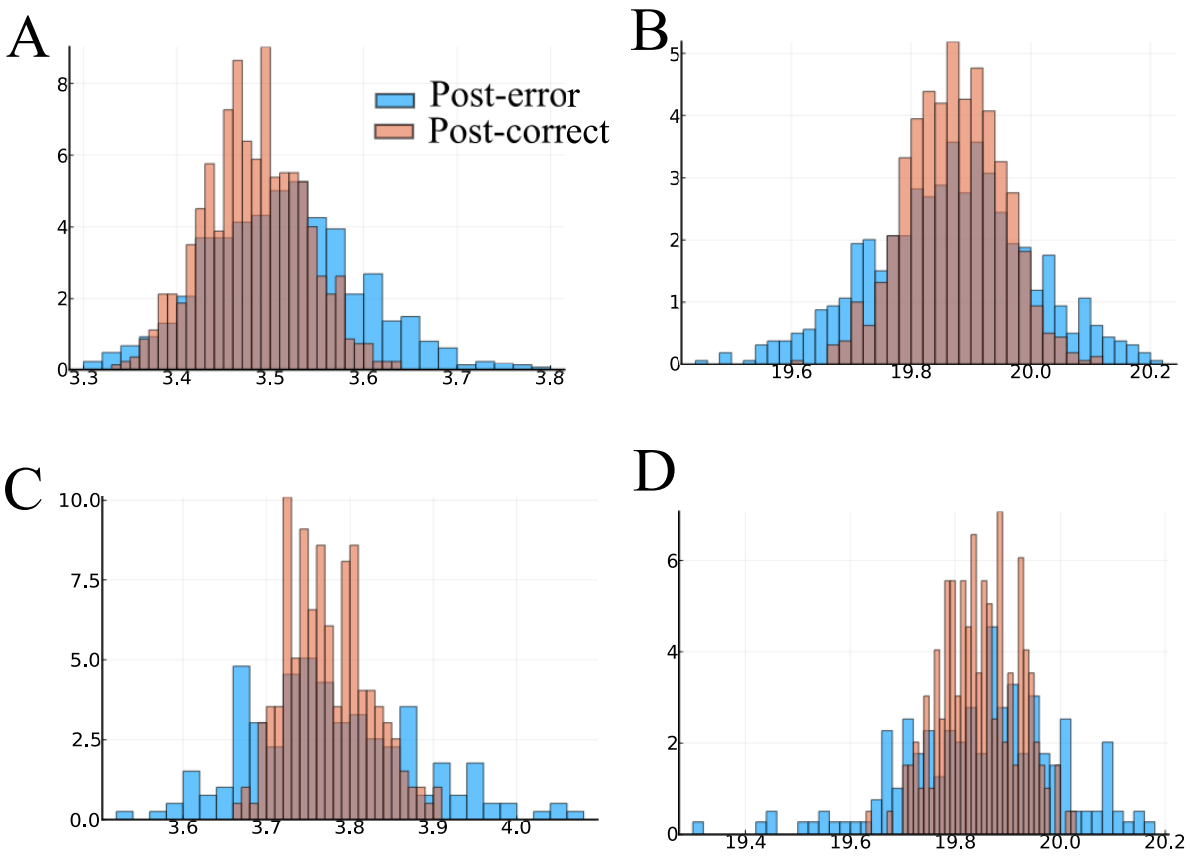

: **Table 2-1: Firing rates distributions at the time of decision.** *(A) and (C): Distribution of the firing rates, at the time of decision, of the losing population. Each histogram represents a different RSI:* 500 *ms for (A) and* 2000 *ms for (C). (B) and (D): Distribution of the firing rates, at the time of decision, of the winning population. Each histogram represents a different RSI:* 500 *ms for (B) and* 2000 *ms for (D).*

RSI	Winning Population	Losing Population
500 ms	Reject, $p = 9.9 \times 10^{-8}$	Reject, $p = 5.3 \times 10^{-19}$
2000 ms	Reject, $p = 0.0044$	Reject, $p = 0.00067$

: Table 2-2: Table of the results for the Smirnov-Kolmogorov test between the post-error / correct distributions of the firing rates at the time of the decision,with respect to the null hypothesis.